T.C.
ERCIYES UNIVERSITY
GRADUATE SCHOOL OF NATURAL AND APPLIED SCIENCES
DEPARTMENT OF MECHANICAL ENGINEERING

INVESTIGATION OF THERMOHYDRAULIC PERFORMANCE WITH THE USE OF GRAPHENE-IRON OXIDE NANOPARTICLES INCORPORATED PURE WATER-ETHYLENE GLYCOL BASED HYBRID NANOFLUID AND MODIFIED HELICAL INSERTS IN A HEAT EXCHANGER TUBE

Author
Onur Metin MERTASLAN

Supervisor
Asst.Prof. ORHAN KEKLİKCİOĞLU

Master Thesis

July 2023
KAYSERİ

T.C.
ERCIYES UNIVERSITY
GRADUATE SCHOOL OF NATURAL AND APPLIED SCIENCES
DEPARTMENT OF MECHANICAL ENGINEERING

INVESTIGATION OF THERMOHYDRAULIC PERFORMANCE WITH THE USE OF GRAPHENE-IRON OXIDE NANOPARTICLES INCORPORATED PURE WATER-ETHYLENE GLYCOL BASED HYBRID NANOFLUID AND MODIFIED HELICAL INSERTS IN A HEAT EXCHANGER TUBE

Author
Onur Metin MERTASLAN

Supervisor
Asst.Prof. ORHAN KEKLİKCİOĞLU

This work was supported by the Erciyes University Scientific Research Projects Unit with the project code FYL-2023-12679.

July 2023
KAYSERİ

COMPLIANCE WITH SCIENTIFIC ETHICS

I declare that all information in this study has been obtained in accordance with academic and ethical rules. At the same time, as required by these rules and conduct, I declare that I have fully cited and referenced all material and results that are not at the core of this work.

Onur Metin MERTASLAN

imza

The MSc. thesis entitled **“Investigation of Thermohydraulic Performance With The Use of Graphene-Iron Oxide Nanoparticles Incorporated Pure Water-Ethylene Glycol Based Hybrid Nanofluid And Modified Helical Inserts In A Heat Exchanger Tube”** has been prepared in accordance with the Graduate Thesis Proposal and Thesis Writing Guidelines of Erciyes University.

By	**Supervisor**
Onur Metin MERTASLAN	Asst. Prof. ORHAN KEKLİKCİOĞLU
İmza	İmza

Head of Department, Mechanical Engineering

Prof. Dr. Orhan AKANSU

İmza

ACKNOWLEDGEMENTS

Dear Ass. Prof. Orhan Keklikcioglu, Mürüvvet Bozkurt, Nisanur Duman, Murat Kerem Ispir, my family, TÜBİTAK, and TAI,

I am profoundly grateful for the exceptional support and encouragement I have received from each of you during my master's thesis journey. Ass. Prof. Keklikcioglu, your guidance and expertise have been invaluable, shaping the outcome of my research. Mürüvvet, Nisanur, and Murat, your contributions have greatly enhanced the quality of the project. To my loving family, your unwavering belief in me has been a constant source of inspiration. I extend my heartfelt appreciation to TÜBİTAK for the “Bideb 2210-A Yurt İçi Genel Yüksek Lisans Burs Programı” and the 1002 Hızlı Destek program under the contract number of 221-M-687, which have provided vital resources. Lastly, I want to express my gratitude to TAI for the opportunity to work on this project. I am deeply thankful to all of you for your unwavering support, which has played a pivotal role in the successful completion of my master's thesis.

Onur Metin MERTASLAN

July 2023, KAYSERİ

BIR ISI DEĞIŞTİRİCİSİ BORUSUNDA GRAFEN-DEMİR OKSİT NANOPARTİKÜLLERİ İLE OLUŞTURULAN SAF SU-ETİLEN GLİKOL BAZLI HİBRİT NANOAKIŞKAN VE MODİFİYE EDİLMİŞ HELİSEL İÇ ELEMAN KULLANILMASIYLA TERMOHIDROLİK PERFORMANSIN İNCELENMESİ

Onur Metin MERTASLAN

Erciyes Üniversitesi, Fen Bilimleri Enstitüsü
Yüksek Lisans Tezi, Temmuz 2023
Danışman: Dr. Öğr. Üyesi ORHAN KEKLİKCİOĞLU

ÖZET

Bu proje kapsamında, grafen-demir oksit nanopartiküller içeren hibrit nanosıvılar ve modifiye edilmiş helisel iç elemanlar kullanılarak ısı değiştirici tüpünün ısı transfer verimliliğinin artırılması amaçlandı. Nanoakışkanlar, su-etilen glikol karışımına farklı nanopartikül ağırlık oranları eklenerek hazırlandı. Nanoakışkan üzerinde SEM ve Zeta potansiyel analizleri gerçekleştirildi. İç elemanlar, farklı çap ve mesafelerde helisel olarak sargılanmış paslanmaz çelik tellerden oluşmaktadır. Deneyler, belirli bir Reynolds sayısı aralığında türbülanslı akış koşulları altında gerçekleştirildi ve ısı transfer artışını değerlendirmek için termal-hidrolik performans katsayısı (THP) hesaplandı. Sonuçlar, %1,00 hibrit nanosıvı ağırlık oranı, fıçı tipi iç eleman ve 3000 Reynolds sayısı konfigürasyonunun en yüksek THP değerine sahip olduğunu gösterdi. Bu konfigürasyon aynı zamanda %0,75 ve %0,50 ağırlık oranları için de yüksek THP değerlerine sahipti. Öte yandan, %0,50 hibrit nanoakışkan ağırlık oranı, düz yay tipi iç eleman ve 15000 Reynolds sayısı konfigürasyonu en düşük THP değerine sahipti. Genel olarak, tüm konfigürasyonlar, THP değerlerinin 1'i aştığı avantajlı termal-hidrolik performans sergiledi. Bu bulgular, nanoakışkanların termal-hidrolik performansı artırmadaki etkinliğini vurgulamaktadır.

Anahtar Kelimeler: Nanoakışkan, Hibrit, Termal-hidrolik, Grafen-Demir oksit, Isı transfer iyileştirme

INVESTIGATION OF THERMOHYDRAULIC PERFORMANCE WITH THE USE OF GRAPHENE-IRON OXIDE NANOPARTICLES INCORPORATED PURE WATER-ETHYLENE GLYCOL BASED HYBRID NANOFLUID AND MODIFIED HELICAL INSERTS IN A HEAT EXCHANGER TUBE

Onur Metin MERTASLAN

Erciyes University, Graduate School of Natural and Applied Sciences
Master Thesis, July 2023
Supervisor: Asst. Prof. Orhan KEKLİKCİOĞLU

ABSTRACT

In this project, the aim was to improve the heat transfer efficiency of a heat exchanger tube by using hybrid nanofluids with Graphene-Iron oxide nanoparticles and modified helical inserts. The nanofluids were prepared by adding different weight ratios of nanoparticles to a water-ethylene glycol mixture. SEM, and Zeta potential analyses were performed on the nanofluids. The inserts were helically wound stainless steel wires of different diameters and distances. Experiments were carried out under turbulent flow conditions within a specific Reynolds number range, and the thermal-hydraulic performance coefficient (THP) was calculated to assess heat transfer enhancement. The results showed that the configuration with a 1.00% hybrid nanofluid weight ratio, barrel coil insert, and Reynolds number of 3000 achieved the highest THP value. This configuration also exhibited high THP values for the 0.75% and 0.50% weight ratios. On the other hand, the configuration with a 0.50% hybrid nanofluid weight ratio, flat coil insert, and Reynolds number of 15000 had the lowest THP value. Overall, all configurations showed advantageous thermal-hydraulic performance, with THP values exceeding 1. These findings highlight the effectiveness of nanofluids in enhancing thermal-hydraulic performance.

Keywords: Nanofluid, Hybrid, thermal-hydraulic, Graphene-Iron oxide, Heat Transfer enhancement

TABLE OF CONTENT

INVESTIGATION OF THERMOHYDRAULIC PERFORMANCE WITH THE USE OF GRAPHENE-IRON OXIDE NANOPARTICLES INCORPORATED PURE WATER-ETHYLENE GLYCOL BASED HYBRID NANOFLUID AND MODIFIED HELICAL INSERTS IN A HEAT EXCHANGER TUBE

COMPLIANCE WITH SCIENTIFIC ETHICS ii

COMPLIANCE WITH DIRECTIVE iii

ACCEPTANCE AND APPROVEL iv

ACKNOWLEDGEMENTS v

ÖZET vi

ABSTRACT vii

TABLE OF CONTENT viii

ABBREVIATIONS xi

LIST of TABLES xiii

LIST of FIGURES xiv

INTRODUCTION 1

1. CHAPTER

GENERAL INFORMATION and LITERATURE REVIEW

1.1.Problem Status 2

1.1.1. Heat Exchangers 2

1.1.1.1. The classification of heat exchangers based on their structural characteristics 2

1.2.Purpose and Importance of the Research, ... 5

1.3.Methods of Enhancement of Heat Transfer 7

1.4.Nanoparticles 8

1.4.1.Nanoparticle Types 10

1.4.1.1.Carbon Based-Nanoparticles 10

1.4.1.2.Ceramic Nanofluids 10

1.4.1.3.Metal Nanoparticles 10

1.5.Literature Review 11

2. CHAPTER

METHOD AND MATERIAL

2.1. Experimental Setup 17

2.2.Experimental Methodology 17

2.3.Preparation of Nanofluids 19

2.4.Determination of the Properties of Nanofluids 21

2.5.Inserts 22

2.6.Calculating Dimensionless Performance Parameters 23

2.6.1.Calculating the Nusselt Number 24

2.6.2.Calculation of Friction Factor 27

2.6.3.Calculation of Thermal and Hydraulic Performance Criteria 27

2.7.Uncertainty Analysis 28

3. CHAPTER

FINDINGS

3.1.Findings Related to The Synthesis of Hybrid Nanofluids 30

3.2.Findings on Thermophysical Properties 31

3.2.1.Regarding the Verification of the Experimental Systematic 32

3.2.2.Findings related to the use of hybrid nanofluid and modified inserts: 32

4. CHAPTER

DISCUSSION-RESULT and SUGGESTIONS

4.1.Discussion 40

4.2.Results and Suggestions.....41

REFERENCES.....44

APPENDICES.....51

APPENDIX 1.....51

RESUME.....52

ABBREVIATIONS

HEXs: Heat Exchangers

PHEs: Plate heat exchangers

CNTs: Carbon nanotubes

MWCNTs: Multi-walled carbon nanotubes

SWCNTs: Single-walled carbon nanotubes

Al: Aluminum

O: Oxygen

Ti: Titanium

Cu: Copper

Si: Silicon

Zn: Zinc

Fe: Iron

GnP: Graphene nanoplatelets

EG: Ethylene Glycol

DC: Direct Current

SDBS: Sodium Dodecylbenzene Sulfonate

ERUTAUM: Erciyes University Technology Research and Application Center

SEM: Scanning Electron Microscopy

ERNAM: Erciyes University Nanotechnology Research Center

Nu: Nusselt Number

f: Friction factor

THP: Thermo-hydraulic performance

Re: Reynolds number

Ra: Rayleigh number

Gr: Grashof number

S/N: Signal-to-noise

Subscirpt:

con: conduction

ow: outer wall

s: surface

env: environment

o: outer

i: inner

is: inner surface

iw: inner wall

LIST OF TABLES

Table 1: Technical specifications of graphene and iron oxide nanoparticles 20
Table 2: Error values of the measured parameters 28
Table 3: Uncertainty analysis values of the experimental data 29

LIST OF FIGURES

Figure 1: Classifcation of HEXs [4] 3
Figure 2:Classifcation of HEXs according to construction [2,4] 3
Figure 3:Schematic of a shell and tube heat exchanger [6] 4
Figure 4: Schematic of a PHEs [8] 5
Figure 5: Schematic of Extended surface HEXs [9] 5
Figure 6: Examples of visual representations for the use of passive method elements in heat exchangers 6
Figure 7: Circular cross-section helical coiled insert 7
Figure 8: Different tube surfaces [35] 9
Figure 9: Different Heat Transfer Enhancement Surfaces [40] 9
Figure 10:Examples of helically coiled inner element used in the studies mentioned in the literature [68-70] 16
Figure 11: Experimental Set-up 18
Figure 12:The schematic structure of the experimental setup. 19
Figure 13:Nanofluid Preparation Diagram 20
Figure 14: Nanofluid preparation and thermophysical property measurement equipment 21
Figure 15: (a) Ultrasonic mixer and (b) pH meter 21
Figure 16: Thermal conductivity measurement diagram and (b) Viscosity measurement diagram [83] 22
Figure 17: (a) SEM device, (b) Zeta Potential (Zetasizer) device. 22
Figure 18: Configurations of internally generated components within the scope of the project 23
Figure 19: The internally generated components and their physical properties within the scope of the project 23
Figure 20: Cross-sectional view of the test tube. 24
Figure 21: SEM image of graphene-iron oxide hybrid nanoparticle 30
Figure 22:Zeta potential distributions of graphene-iron oxide hybrid nanoparticle 31

Figure 23: (a)Verification of thermal conductivity measurements (b) Verification of viscosity measurements with literature (ASHRAE [80])..... 33
Figure 24:Variation of (a) thermal conductivity coefficients and (b) viscosity values with temperature for three different hybrid nanofluid weight ratios..... 34
Figure 25:Comparison of the variation of (a) Nusselt number and (b) friction factor with Reynolds number obtained from empty tube experiments with the literature..... 35
Figure 26: Distribution of Nusselt number with respect to Reynolds number for (a) 0.50%, (b) 0.75%, and (c) 1.00% hybrid nanofluid weights in insert usage..... 36
Figure 27:Distribution of friction factor with respect to Reynolds number for (a) 0.50%, (b) 0.75%, and (c) 1.00% hybrid nanofluid weights in insert usage..... 37
Figure 28:Distribution of thermo-hydraulic performance coefficient with respect to Reynolds number for (a) 0.50%, (b) 0.75%, and (c) 1.00% hybrid nanofluid weights in insert usage..... 38

INTRODUCTION

Currently, there is an increasing trend towards alternative and renewable energy sources worldwide, including solar energy, wind energy, biomass energy, geothermal energy, marine energy, and waste-to-energy, to meet the growing energy demand. This trend is also evident in Turkey, where notable policies have been implemented. Despite government support and investor incentives, the cost of renewable energy sources remains relatively high, although it is expected to decrease shortly [1]. In this regard, the widespread adoption of current and technological engineering products in our country is directly related to their cost. Therefore, maximizing the utilization of systems that utilize renewable and alternative energy sources in Turkey will require the implementation of economic systems. In light of this data, it is more important to focus on efficient energy use and reducing energy losses through engineering methods such as updates to high-energy-consuming systems to make them more energy-efficient, rather than just diversifying energy sources. It is crucial to ensure the control of energy consumption from existing energy sources and to preserve technical values such as system efficiency, performance, and component lifespan, regardless of whether renewable or alternative energy sources are used.

This project involves conducting experimental research on thermal-hydraulic performance by introducing modified inserts into a horizontal heat exchanger tube, utilizing a design that has not been explored in previous studies. Furthermore, the study investigates the enhancement of heat transfer by introducing Graphene-Iron oxide nanoparticles into a water-ethylene glycol mixture, serving as the base fluid, at various mixing ratios through the use of hybrid nanofluids.

1. CHAPTER

GENERAL INFORMATION and LITERATURE REVIEW

1.1. Problem Status

1.1.1. Heat Exchangers

Heat exchangers (HEXs) are devices designed to facilitate the transfer of thermal energy between two or more fluids with varying temperatures. They utilize a surface to separate the streams of fluids to prevent them from mixing. HEXs find application in various fields, such as air conditioning, cooling of substances that need temperature control, renewable energy technologies, and systems that recover energy [2]. Various criteria have been suggested for classifying heat exchangers (HEXs). Broadly speaking, heat exchangers have been categorized based on their construction, transfer processes, levels of surface compactness, flow arrangements, pass arrangements, phase of the process fluids, and heat transfer mechanisms [3].

1.1.1.1.The classification of heat exchangers based on their structural characteristics

The classification of heat exchangers based on their structural characteristics, as shown below, has been classified by Shah et al. [4].

In a shell and tube heat exchanger, there are two fluids with different temperatures that pass through the exchanger. One fluid flow through the tubes (known as the tube side), while the other flows outside the tubes within the shell (known as the shell side). Heat is exchanged between the fluids through the walls of the tubes, either from the tube side to the shell side or vice versa. Both the shell and tube sides can accommodate either liquids or gases. To ensure effective heat transfer, a large surface area is utilized, which involves the use of numerous tubes. This design promotes energy efficiency and minimizes thermal energy waste [5].

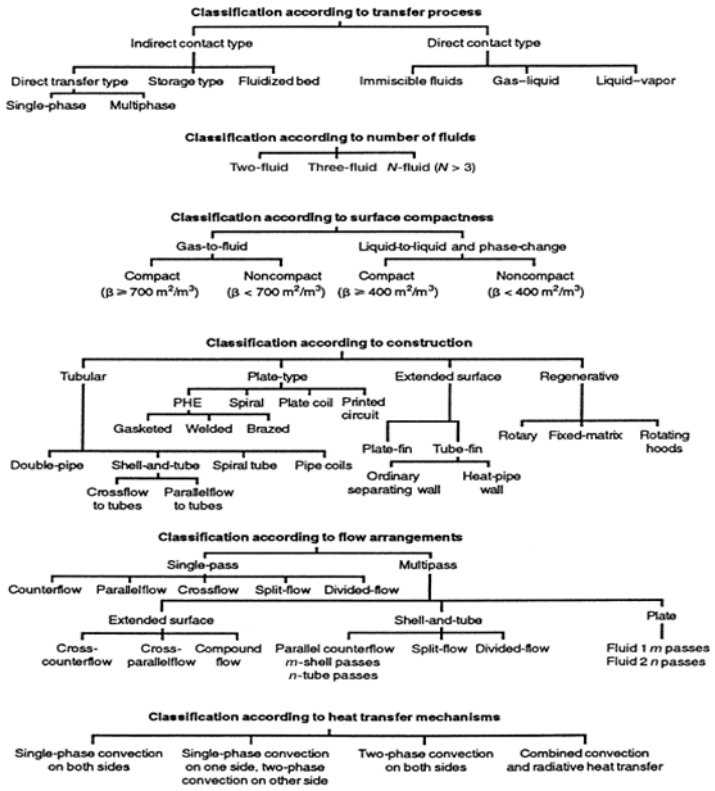


Figure 1: Classifcation of HEXs [4]

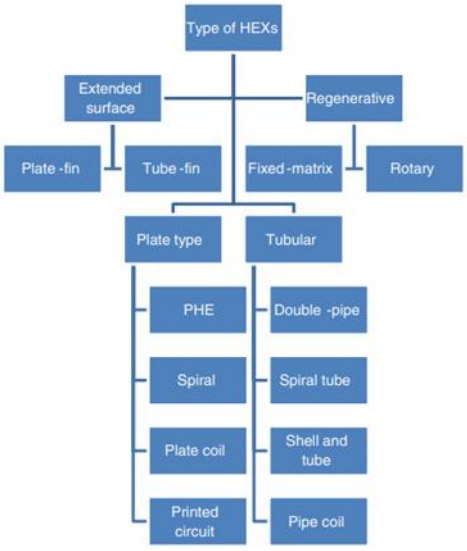


Figure 2:Classifcation of HEXs according to construction [2,4]

In a shell and tube heat exchanger, there are two fluids with different temperatures that pass through the exchanger. One fluid flows through the tubes (known as the tube side), while the other flows outside the tubes within the shell (known as the shell side). Heat is exchanged between the fluids through the walls of the tubes, either from the tube side to the shell side or vice versa. Both the shell and tube sides can accommodate either liquids

or gases. To ensure effective heat transfer, a large surface area is utilized, which involves the use of numerous tubes. This design promotes energy efficiency and minimizes thermal energy waste [5].

Plate heat exchangers (PHEs) find widespread usage in the chemical, food, and pharmaceutical industries for purposes such as heating, cooling, and heat regeneration. Initially, these exchangers were specifically developed for hygienic applications like pasteurizing liquid food products. However, over the past few decades, significant advancements in design and construction have greatly broadened the range of applications for this type of heat exchanger. The plate heat exchanger (PHE) is composed of a collection of corrugated metal plates tightly pressed within a frame. The presence of gaskets between these plates creates a network of narrow channels where the hot and cold fluids flow, allowing for heat exchange via the metal plates. The distribution of flow within the plate pack is determined by various factors, including the gasket design, the open and closed ports of the plates, and the positioning of the feed connections located at the covers [7].

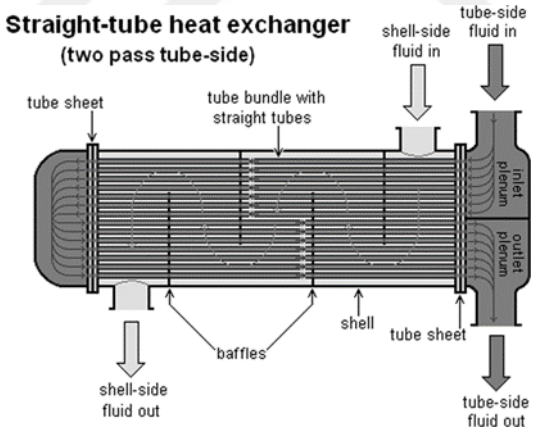


Figure 3:Schematic of a shell and tube heat exchanger [6]

Extended surface heat exchangers are used to increase the areas by structures such as Fins. Fins are primarily used to increase the overall surface area, especially when the heat transfer coefficient on that particular fluid side is relatively low. This increase in surface area subsequently enhances the total heat transfer rate. Furthermore, these extended fin geometries also contribute to higher heat transfer coefficients compared to plain fins. Fins can also be employed on the side with a higher heat transfer coefficient in a heat exchanger for reasons such as providing structural strength, such as for high-pressure

water flow through a flat tube, or promoting thorough mixing of highly viscous liquids, as seen in laminar oil flow through a flat or round tube [9].

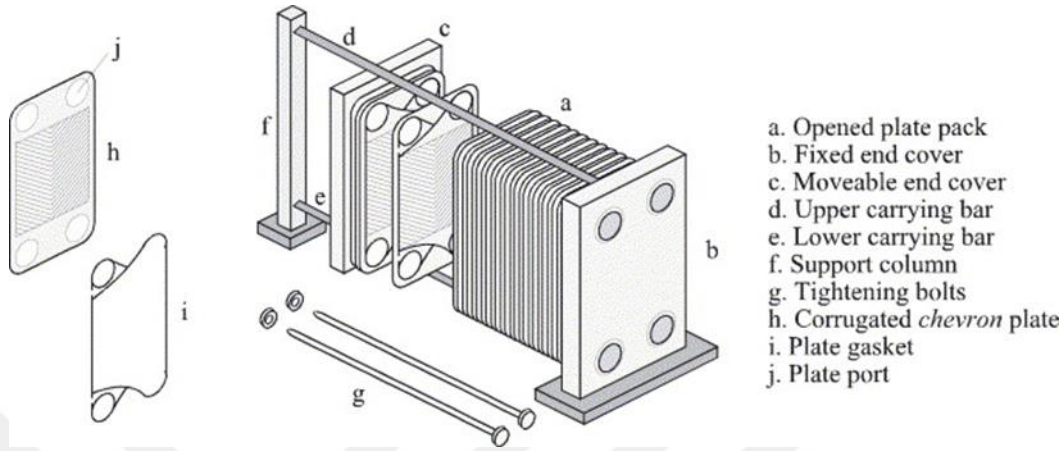


Figure 4: Schematic of a PHEs [8]

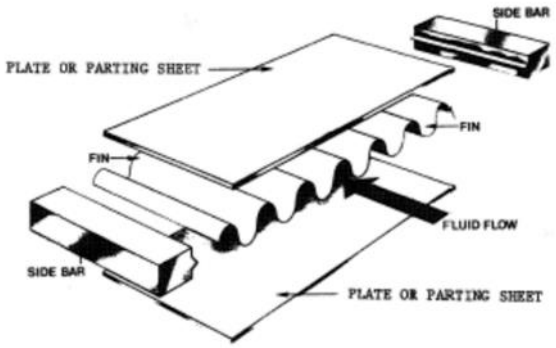


Figure 5: Schematic of Extended surface HEXs [9]

1.2. Purpose and Importance of the Research,

Temperature control in complex engineering systems not only enhances the efficient utilization of energy but also extends the lifespan of the system as a whole or its individual components while ensuring operational stability. Improving the performance of heat exchangers, which are one of the most commonly used engineering systems for temperature control, directly impacts the overall efficiency of the connected system. Therefore, any technical enhancements that increase the heat transfer capability of the heat exchanger are highly valuable from both practical and scientific perspectives. In this context, researchers conduct various studies to enhance the heat transfer capabilities of heat exchangers. These studies primarily focus on techniques known as passive methods, which are easy to install, require minimal maintenance, do not rely on external energy

input, and aim to design more efficient heat exchangers. Passive methods for improving heat transfer, as shown in Figure 1, involve the placement of different inserts within the heat exchanger tube to create flow disturbances and blockages, thereby achieving higher rates of heat transfer. One of the best examples of this method is the use of helically coiled inserts, as illustrated in Figure 2, which not only enhance heat transfer but also result in lower pressure drop compared to other types of inserts, negatively impacting the efficiency of the system [10].

In addition to studies focused on enhancing the thermal efficiency of heat exchangers through passive methods, the use of nanofluids in heat exchangers has rapidly gained popularity in recent years, along with the adaptation of nanotechnological engineering applications to complex systems. It is notable that nanofluids, which contain nanoparticles, are being increasingly used in heat exchangers instead of conventional heat transfer fluids such as water, monoethylene glycol, propylene glycol, and oil.



Figure 6: Examples of visual representations for the use of passive method elements in heat exchangers

The primary objective of applying nanoparticles in base fluid types is to increase the average heat transfer coefficient of the fluid by introducing particles with a solid-phase structure and high thermal conductivity into the fluid. This objective aims to extract thermal loads from the systems or enable the recycling of thermal loads, thereby reducing heat loss. Additionally, the addition of solid particles to the fluid not only enhances the fluid's thermal conductivity but also contributes to the formation of turbulence within the flow, increases the surface area, improves the micro-transport characteristics through particle-particle collisions, and consequently enhances the heat transfer rate. Therefore, it is of great importance to investigate and implement technological advancements to improve the performance of heat exchangers, which play a crucial role in numerous engineering applications.

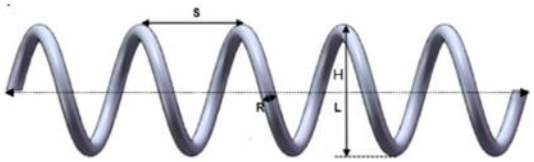


Figure 7: Circular cross-section helical coiled insert

1.3. Methods of Enhancement of Heat Transfer

In general, techniques for enhancing heat transfer aim to decrease thermal resistance by either increasing the effective surface area for heat transfer or promoting turbulence in the fluid passing through the device [11]. In general, when heat transfer is enhanced, it often comes at the expense of increased pressure drop, resulting in higher energy requirements for pumping. Researchers have been striving to develop techniques that can enhance heat transfer while minimizing the associated pressure drop. These techniques involve the forced flow of various fluids, such as air, water, mineral oil, ethylene glycol, and nanofluids, over the heated surface. The characteristics of the heated surface, such as smoothness, roughness, stationarity, or movement, depend on the specific applications. Heat transfer enhancement methods are typically categorized as either active or passive methods [12, 13, 14].

Active methods of heat transfer enhancement require an external power source and generally result in a greater increase in heat transfer compared to passive methods. These active methods are preferred when it is important to maintain the simplicity and original design of the heat exchanger [15]. Due to the requirement of additional equipment, increased complexity and cost make them less commonly used. In contrast to passive techniques, these methods have not demonstrated significant potential, as it can be challenging to supply external power input in various scenarios [16, 17]. Electroactive material [18], Electrohydrodynamic [19,20], Magnetic materials [21], Jets, Spray [22], Mechanical aids [23], Surface vibration [24], Flow-induced vibration [25] and Ultrasonic vibration [26] can be given as examples of active methods.

The heat exchanger industry has been working towards enhancing thermal contact (increasing heat transfer coefficient) and minimizing pumping power to improve the overall thermohydraulic efficiency of heat exchangers. An effective heat exchanger design should exhibit efficient thermodynamic performance. Passive methods, which do

not require external power, typically involve modifying the geometry or surface of the flow tube through additional devices or inserts. By altering the flow characteristics, these methods enhance the heat transfer rate, albeit at the expense of increased pressure drop [17,27,28]. There are several methods such as porous materials [29-31], inserts such as turbulators, wire coils, swirl flow tools, and twisted strips [32-34], rough surfaces like corrugated surfaces [35,36], extended surfaces like fins, dimples, and protrusions [37-41], the use of nanofluids [42-47], displaced enhancement devices, and more.

1.4. Nanoparticles

Nanofluids are defined as fluids in which nanometer-sized particles are dispersed within conventional heat transfer fluids. Conventional heat transfer fluids such as oil, water, and ethylene glycol mixtures have limited heat transfer capabilities due to their low thermal conductivity, which affects the heat transfer coefficient between the heat transfer medium and the surface. To address this limitation, various methods have been employed to enhance the thermal conductivity of these fluids by incorporating suspended nano/micro or larger-sized particles in the liquid medium [48]. The incorporation of solid nanoparticles, which typically have high thermal conductivity and range in size from 1 to 100 nm, into base fluids with low thermal conductivity has been found to enhance the effective thermal conductivity and convective heat transfer coefficient of the base fluid. Nanoparticles made of materials such as Al_2O_3, CuO, Cu, SiO, and TiO, whether metallic or nonmetallic, exhibit thermal conductivities that are typically an order of magnitude higher than those of the base fluids, even at low concentrations. As a result, nanofluids demonstrate significant increases in the heat transfer coefficient leading to enhanced heat transfer compared to conventional heat transfer liquids [44,48,49].

The incorporation of solid nanoparticles, which typically have high thermal conductivity and range in size from 1 to 100 nm, into base fluids with low thermal conductivity has been found to enhance the effective thermal conductivity and convective heat transfer coefficient of the base fluid. Nanoparticles made of materials such as Al_2O_3, CuO, Cu, SiO, and TiO, whether metallic or nonmetallic, exhibit thermal conductivities that are typically an order of magnitude higher than those of the base fluids, even at low concentrations. As a result, nanofluids demonstrate significant increases in the heat

transfer coefficient leading to enhanced heat transfer compared to conventional heat transfer liquids [44,48,49].

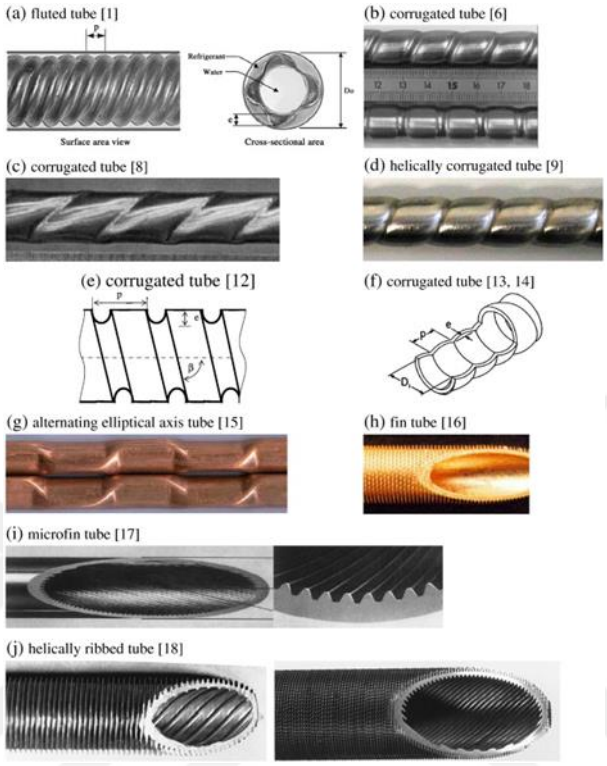


Figure 8: Different tube surfaces [35]

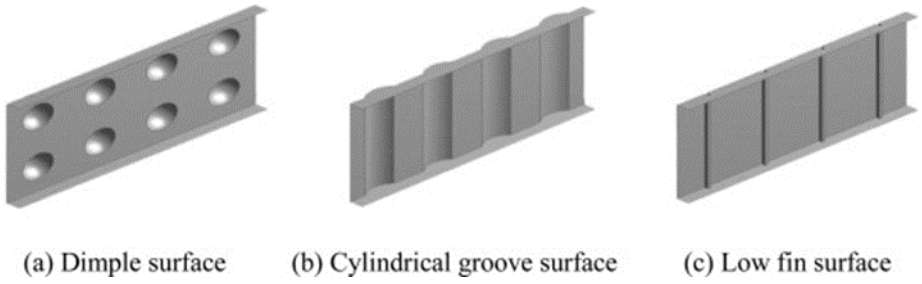


Figure 9: Different Heat Transfer Enhancement Surfaces [40]

Advantages of nanofluids can be listed as follows:

- The inclusion of nanoparticles in the fluid leads to an increase in both the fluid's surface area and heat capacity.
- The incorporation of nanoparticles in the fluid results in an augmentation of the fluid's effective thermal conductivity.
- The presence of nanoparticles intensifies the interaction and collision between particles, fluid, and the surface of the flow passage.

- The presence of nanoparticles enhances the mixing fluctuations and turbulence within the fluid.
- The dispersion of nanoparticles aids in reducing the transverse temperature gradient of the fluid [44].

1.4.1. Nanoparticle Types

Nanofluids exhibit significantly enhanced thermal conductivity in comparison to regular suspensions. The increase in thermal conductivity of nanofluids surpasses that of micrometer-sized suspensions by several times. Commonly employed base fluids include water, ethylene glycol, transformer oil, and toluene. The categorization of nanoparticles can be based on their size, shape, as well as their physical and chemical characteristics. Frequently, this classification plays a significant role in determining the specific roles and functions of these nanomaterials [50-51].

1.4.1.1.Carbon Based-Nanoparticles

Mainly, carbon-based nanoparticles are divided into two categories: carbon nanotubes (CNTs) and fullerenes. These nanoparticles are primarily utilized for enhancing structural integrity due to their remarkable strength, which is approximately 100 times greater than that of steel.

CNTs can be further classified into two types: single-walled carbon nanotubes (SWCNTs) and multi-walled carbon nanotubes (MWCNTs). What sets CNTs apart is their distinctive thermal conductivity along the length of the tube while being non-conductive across the tube [50-51].

1.4.1.2.Ceramic Nanofluids

Inorganic solid nanoparticles, encompassing oxides, carbides, carbonates, and phosphates, fall under the category of ceramic nanoparticles. These nanoparticles possess excellent heat resistance and chemical inertness, making them well-suited for various applications such as photocatalysis, dye photodegradation, and biological imaging [50].

1.4.1.3.Metal Nanoparticles

Metal nanoparticles are a class of nanoparticles derived from metal precursors and can be synthesized through chemical, electrochemical, or photochemical means. Chemical methods involve the reduction of metal-ion precursors in a solution using chemical reducing agents to obtain the desired metal nanoparticles. These resulting nanomaterials exhibit properties such as the ability to adsorb small molecules and possess high surface energy. The most frequently encountered metal nanoparticles include silver, gold, palladium, titanium, zinc, and copper nanoparticles [50-51].

1.5. Literature Review

The importance of the passive approach becomes evident when we consider the thermal-hydraulic performance. In industrial settings, enhancing thermal contact and minimizing energy consumption for pumping are essential factors for improving efficiency and cost-effectiveness when designing heat exchangers. For these reasons, a wide range of methods have been implemented for thermal enhancement. Among them, passive methods are the most commonly used. Combinations of passive methods have also gained significant prominence in recent times. For example, the utilization of nanoparticles or the introduction of hybrid nanoparticles, alongside inserts, is being employed. The use of nanofluids obtained by dispersing nanoparticles in base fluids has increased in studies focused on improving heat transfer, as these nanofluids exhibit enhanced thermophysical properties compared to Commonly encountered fluids like water, oil, and ethylene glycol can be described as traditional fluid substances. Various types of nanoparticles, including metals (such as Al_2O_3, TiO_2, CuO, SiO_2, ZnO), oxides, and carbon nanotubes (such as graphene oxide, Fe_3O_4, GnP), have been utilized in these studies. In a study conducted by Chen et al. [52], a comparison was made between a standard smooth tube and six dimpled copper tubes with varying geometries. The tube with the largest structural value, Tube 4, exhibited the highest enhancement in heat transfer coefficient at 2.37 times that of the smooth tube. The dimpled tubes demonstrated larger heat transfer coefficients, ranging from 1.25 to 2.37 times, and showed improved performance across the Reynolds number range. The Reynolds number exponent varied from 0.883 to a maximum of 0.934. The effectiveness of dimpled tubes as enhancement devices was observed at both low and high flow rates. The friction factor for all the dimpled tubes was found to be 1.08 to 2.35 times higher compared to the smooth tube. The study showed that the augmentation in heat transfer ranged from 1.25 to 2.37 times at a constant Reynolds number, and from

1.15 to 1.84 times at a constant pumping power. Piper et al. [53] conducted a numerical study on pillow-plate heat exchangers with dimpled surfaces. The numerical findings revealed that the presence of dimples resulted in an increased number of recirculation zones. However, these zones were smaller and less energetic. Additionally, the dimples caused regular disruptions in the turbulent boundary layer, thereby enhancing mixing near the wall. Consequently, there was a 2.2% increase in the heat transfer coefficient. Simultaneously, the pressure loss in the modified channel decreased by 8.7%. Overall, the thermo-hydraulic efficiency in the new channel experienced an 11.2% enhancement compared to traditional pillow plates.

Xuan et al. [44] provide evidence that the thermal conductivity of nanofluids can be determined using the hot-wire method. The results obtained from the measurements demonstrate a significant increase in the thermal conductivity of nanofluids as the volume fraction of ultrafine particles increases. For instance, in the case of a water-Cu nanoparticles suspension, the ratio of the thermal conductivity of the nanofluid to that of the base liquid ranges from 1.24 to 1.78 when the volume fraction of the ultrafine particles rises from 2.5% to 7.5%. Zamzamian et al. [45] conducted a study on the utilization of nanofluids containing Al_2O_3/EG and CuO/EG in both double pipe and plate heat exchangers operating under turbulent flow conditions. The results showed that in the double pipe heat exchanger, the maximum heat transfer enhancement achieved was 26% when using 1.0% weight of aluminum oxide in ethylene glycol, and 37% when using 1.0% weight of copper oxide in ethylene glycol. In the plate heat exchanger, these enhancements were even higher at 38% and 49%, respectively. Hussein et al. [47] conducted a study to measure the forced convection heat transfer enhancement using TiO_2 and SiO_2 suspended in water as the base fluid in flat copper tubes of an automotive cooling system. The research revealed a substantial enhancement in heat transfer, which was directly related to the concentration of nanoparticles. The maximum enhancements in Nusselt numbers reached up to 11% for TiO_2 nanoparticles and 22.5% for SiO_2 nanoparticles when suspended in water.

Although numerous scientific studies have been conducted in recent years on the subject of heat transfer using nanoparticles, no research has been carried out to enhance heat transfer using a modified helical insert combined with a Graphene-Iron Oxide hybrid nanoparticle. In this regard, existing literature has been reviewed to summarize the

applied techniques. Among the particles investigated for heat transfer, Graphene nanoparticles have been widely studied due to their high thermal conductivity (approximately 3000W/mK) compared to other metal oxides and metal nanoparticles, as well as their superior stabilization ability. Therefore, Graphene nanoparticles have been proposed as the primary particle to be used in the thesis project [54]. On the other hand, Iron Oxide nanoparticles, which exhibit magnetic properties and have been extensively used in various fields such as chemistry, mechanics, pharmaceuticals, electromagnetic applications, and biomedicine in conjunction with Graphene nanoparticles [55-59], have been chosen as the preferred secondary metal-oxide nanoparticle, despite not being used in a hybrid form with an insert for heat transfer enhancement studies.

Research studies on the thermal and hydraulic performance of nanofluid utilization began to diversify in 2017. Studies involving the hybrid use of Graphene nanoparticles with different particles and the incorporation of an insert within the area of Graphene-based nanofluids have been conducted exclusively after 2017. Among these studies, Askari et al. [60] performed an experimental investigation in 2017. They added Fe_3O_4/Graphene nanoparticles individually and in hybrid form at weight fractions of 0.1, 0.2, and 1.0 to a water-based fluid under laminar flow conditions with Reynolds numbers ranging from 2000 to 5000. The thermal properties of the flow inside a smooth tube were determined. The results showed an enhancement in thermal conductivity ranging from 14% to 32% compared to the base fluid. Furthermore, at a Reynolds number of 4248, an increase of 8.5% in heat transfer coefficient was observed for the Iron Oxide-water nanofluid and 14.5% for the Iron Oxide/Graphene hybrid nanofluid. These findings demonstrate the progress made in the field of nanofluid utilization in 2017. In another study, Yarmand et al. [61] conducted an experiment in 2017 using a hybrid combination of Graphene nanoparticles and Platinum nanoparticles. They reported a 28.48% enhancement in Nusselt number compared to the results obtained using a nanofluid with only Graphene nanoparticles, at a Reynolds number of 17,500 and a weight concentration of 0.1%. The authors stated that this enhancement was a result of the synergistic effect and increased thermal conductivity of the nanocomposite (hybrid) structure. According to the results of the same configuration, there was a 49.16% increase in heat transfer coefficient, attributed to the improved thermophysical properties of the nanocomposite and the effective Brownian motion of the nanofluid.

In their 2019 study, Bahiraei et al. [62] numerically investigated the effects of Graphene and Platinum nanoparticles in a nanofluid on heat transfer using three different configurations of bent strip inserts. They found that using the bent strip inserts in conjunction with the nanofluid resulted in significantly higher efficiency compared to water. The configuration with bent strip inserts placed in opposite directions was reported to have superior heat transfer enhancement compared to other models due to increased turbulence within the flow. In the configuration using a nanofluid with a concentration of 0.1% and a bending ratio of 2.5, the Nusselt number was approximately 2.1 times higher than that of a smooth tube with water as the working fluid. In another study by Bahiraei et al. [63], entropy generation analysis was conducted using a nanofluid with Graphene and Platinum nanoparticles, in combination with bent strip inserts placed in opposite and same directions. The study indicated that the use of a nanofluid instead of a base fluid reduced entropy generation and thus decreased irreversibilities. Furthermore, the use of bent strip inserts in opposite directions was found to better disrupt the boundary layer, resulting in a 10% reduction in entropy generation.

In their recent study, Bahiraei et al. [64] analyzed the enhancement in heat transfer using a graphene-platinum hybrid nanofluid in a concentric tube heat exchanger model, incorporating vertical obstacles. The study indicated that the model with the shortest distance between obstacles, the tallest obstacle height, and the highest hybrid nanofluid mixture ratio exhibited the best performance in terms of heat transfer enhancement. Based on these findings, it can be inferred that studies focusing on the combined use of graphene nanoparticles and iron oxide nanoparticles for heat transfer enhancement are still limited and relatively new. Graphene and iron oxide nanoparticles are commonly used in hybrid form for energy storage and composite material studies. In an article compiled by Wang and Liu [65], the effect of graphene and iron oxide hybrid usage in energy storage was investigated. It was stated that the problems arising from the low stability and conductivity of iron oxide nanoparticles were overcome by the relatively higher stability and conductivity of graphene nanoparticles, and the stability and other thermophysical properties of graphene nanoparticles were also enhanced in the hybrid usage with iron oxide. Another study conducted by Lu et al. [66] highlighted the specific advantages of iron oxide nanoparticles, such as low cost and high abundance compared to other nanoparticles but mentioned that they exhibit weaknesses in terms of low conductivity

and proneness to precipitation. To address these weaknesses, the study emphasized the need to focus on the hybrid usage of graphene nanoparticles, which are characterized by their 2D structure, unique atomic thickness, high surface area, high stability, and superior thermophysical properties. It was emphasized that hybrid structures composed of these nanoparticles should be utilized in various fields. Additionally, the study suggested that the different geometric structures of iron oxide and graphene nanoparticles would provide an additional advantage. It was noted that iron oxide nanoparticles located between graphene nanoparticle plates in the hybrid usage would delay the precipitation of graphene nanoparticles. In another investigation focusing on singular and hybrid nanofluids, Sylwia Wcislik [67] stated that valuable results in terms of thermophysical properties can be achieved by using low-cost nanoparticles in combination with relatively higher-cost nanoparticles in hybrid nanofluid models, thereby overcoming the issue of high cost. The results obtained from these studies suggest that the hybrid usage of graphene and iron oxide nanoparticles can improve parameters such as rapid precipitation and low conductivity associated with iron oxide nanoparticles, while also addressing the cost-related obstacles encountered in the singular usage of graphene nanoparticles.

Helical coiled inner tubes are commonly used as a passive heat transfer enhancement method in heat transfer enhancement studies. In recent years, Akyürek et al. [68] investigated the effect of helically coiled inner tubes on heat transfer in an Al_2O_3-water nanofluid heat exchanger tube. They examined the influence of the inner coil with two different coil pitches in the Reynolds number range of 4000-20,000. According to the study, compared to the results of an empty tube with only water, the use of the inner coil improved the Nusselt number by up to 91.86%. When the helical inner coil was used in conjunction with the nanofluid, it resulted in an enhancement of up to 40.25% in the Nusselt number compared to the nanofluid flow in an empty tube, along with a 10.66% enhancement in the heat transfer coefficient. Abdul Hamid et al. [69] investigated the thermal performance of helical inner coils placed in an ethylene glycol-water mixture flow field with five different coil pitches in the Reynolds number range of 2300-12,000, using TiO_2-SiO_2 nanoparticles. The results indicated a 254% enhancement in heat transfer when using the helical inner coil in conjunction with the nanofluid. K. Goudarzi and H. Jamali [70] conducted an investigation on heat transfer enhancement using helical inner coils and Al_2O_3-ethylene glycol nanofluid in an automotive radiator. The experimental

study involved two different types of helical inner coils, and it resulted in a 9% enhancement in the thermal performance of the radiator due to the use of the inner coil. Hong et al. [71] examined the influence of helical inner coils with uniform and variable coil pitches on heat transfer and flow characteristics in a straight air-filled tube in the Reynolds number range of 6000-20,000. The study concluded that helical inner coils with a uniform coil pitch achieved higher heat transfer enhancement coefficient values compared to those with variable coil pitches.

The helical coiled inner element can effectively disrupt the laminar boundary layer compared to other inner elements. Due to its geometry, it causes more flow disturbances inside the tube and results in a lower pressure drop [60]. On the other hand, the helical inner element has a lower impact on pump power compared to other inner elements. Therefore, the utilization of a hybrid nanofluid-helical inner element system in pipe flow applications aims to improve heat transfer performance while keeping the increase in pump power at a minimum compared to other systems. Based on the reviewed studies, there is only one study in the literature that investigates the hybrid use of graphene nanoparticles with iron oxide in heat transfer studies. Upon examining other conducted studies, it is evident that they predominantly consist of numerical modeling and analysis studies based on experimental investigations, carried out by specific research groups.

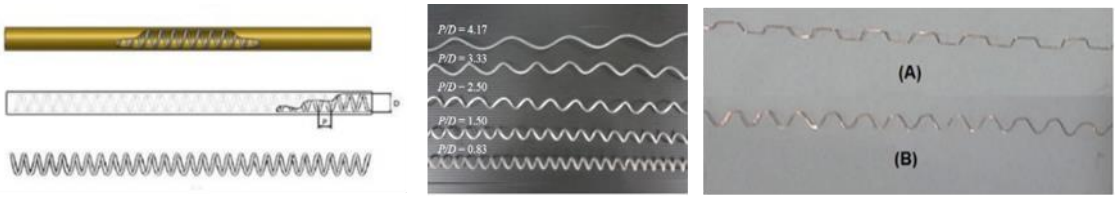


Figure 10:Examples of helically coiled inner element used in the studies mentioned in the literature [68-70]

When examining the helical coiled inner element models as shown in Figure 10, it can be observed that the conducted studies include the traditional coil-type model and limited configurations are created solely by altering the coil ratios. It is noteworthy that the helically coiled inner elements are used without undergoing any modifications.

2. CHAPTER

METHOD AND MATERIAL

2.1. Experimental Setup

The experiments conducted for the project were performed utilizing the experimental arrangement shown in Figure 11, which is situated in the Thermodynamics Laboratory of the Department of Mechanical Engineering within the Faculty of Engineering at Erciyes University.

The experimental configuration illustrated in Figure 11 comprises several components: a fluid tank that allows the fluid to be transferred to the suction line through gravitational force, a mono pump carefully selected to ensure smooth operation and minimize instantaneous pressure differences, regulated by a frequency inverter to facilitate fluid movement within the system, a hydrodynamic development tube made of seamless stainless steel (SS-304) with dimensions of 1000 mm length, 17 mm inner diameter, and 21 mm outer diameter, intended to enhance the hydrodynamic development of the fluid before entering the experimental tube [72], an experimental tube and an outlet tube made of the same material and having identical diameter, measuring 1100 mm and 500 mm in length, respectively, a cooling unit positioned at the outlet to cool the fluid to room temperature, a variable transformer system with a power rating of 10.5 kVA to maintain a constant surface flow rate in the experimental tube, current and voltage meters for measurement purposes, a differential pressure gauge connected to the inlet and outlet points of the experimental tube to measure pressure differences, a flowmeter installed on the outlet tube to measure the flow rate, a total of 23 K-type thermocouples, including 20 placed on the experimental tube, one in the fluid tank, and one in the external environment, a data logger for collecting data, and a computer for data processing.

2.2. Experimental Methodology

As depicted in Figure 12, the fluid undergoes flow development within the flow development tube before entering the test tube. The fluid is first introduced into the test tube, where valves at the inlet and outlet are connected to the DC current cables from the variable transformer and the transformer. This connection creates a short circuit to ensure a consistent heat flux for heating. The current intensity supplied to the system is measured using a current meter through which the cables passing through the test tube are routed. Similarly, the voltage value supplied to the system is measured by connecting a multimeter to the cables leading to the test tube, allowing the power supplied to be calculated in watts. On the outer surface of the tube, two pairs of thermal elements (thermocouples) are strategically placed at 10 cm intervals. This arrangement enables the measurement of local radial temperatures on the tube's outer surface. The thermal element pairs are positioned on both the upper and lower surfaces of the tube, ensuring that any temperature discrepancies are monitored. Furthermore, after the test tube, one pair of thermal elements is immersed into the outlet tube before the flow meter to measure the temperature of the fluid at the exit point. Inside the collection tank, one pair of thermal elements is submerged in the fluid to measure the temperature at the inlet, while another pair is positioned in the ambient environment to measure the surrounding temperature. To minimize heat dissipation from the heated test tube to the surroundings, the test tube is insulated with stone wool material.

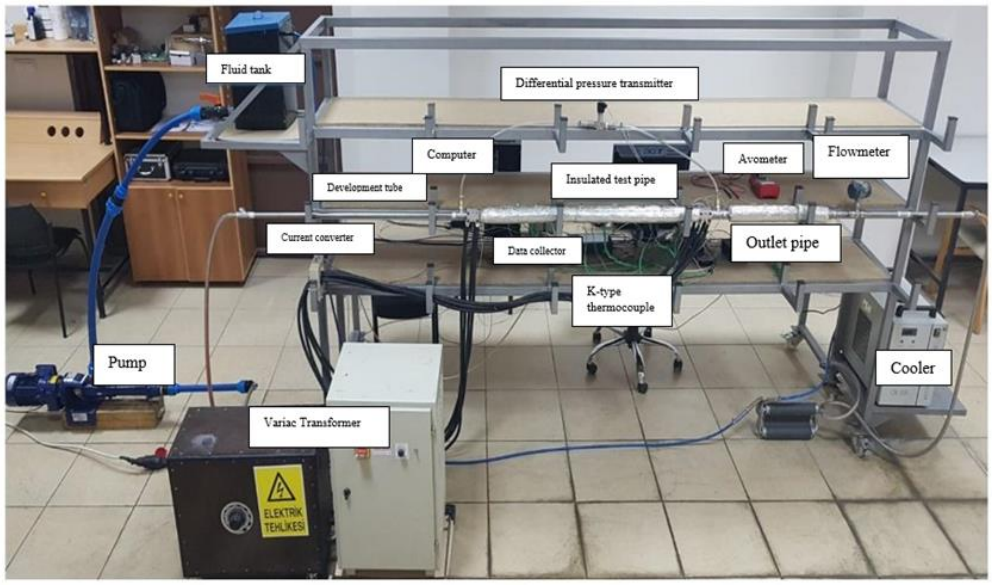


Figure 11: Experimental Set-up

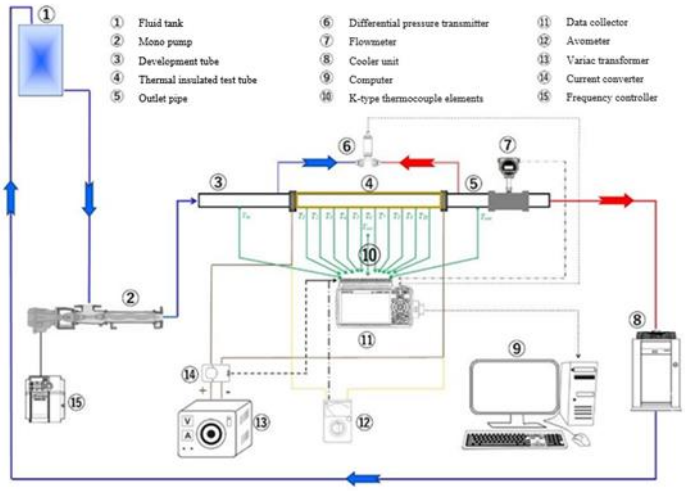


Figure 12:The schematic structure of the experimental setup.

In order to assess the performance of the insert within the tube, pressure taps have been installed at the inlet and outlet of the test tube, as illustrated in Figure 12. These pressure taps are connected to a differential pressure gauge device via a transparent hose, allowing for the measurement of pressure drop along the test tube. Once the fluid exits the test tube, it flows through the outlet tube. To determine the flow rate of the fluid at this stage, a turbine-type flowmeter is utilized. The use of the outlet tube before the flowmeter ensures that temperature and pressure measurements within the test tube remain unaffected. The heated fluid, which flows through a pipeline made of chrome materials, is directed to the collection tank through a hose. To maintain a continuous cycle within the experimental setup, the temperature of the fluid entering the collection tank needs to be reduced to the initial room temperature condition. To achieve this, a cooling unit and heat exchanger are employed to cool the fluid down to room temperature.

2.3. Preparation of Nanofluids

During the study, nanofluids were created by incorporating Graphene-Iron oxide nanoparticles into a base fluid composed of 80% pure water and 20% ethylene glycol, at three different weight proportions (0.5%, 0.75%, 1%). The characteristics of the Graphene and Iron oxide nanoparticles can be found in Table 1. The nanofluids were prepared following a two-step method [73,74] at the designated weight ratios.

During the initial phase of the nanofluid preparation process, a surfactant was introduced into the base fluid and subjected to mechanical mixing. Subsequently, the nanoparticles

were added to the mixture of base fluid and surfactant, according to the specified weight ratios, and mixed once again using a mechanical mixer. Following the mechanical mixing step, the nanofluid mixture underwent ultrasonic mixing.

Table 1: Technical specifications of graphene and iron oxide nanoparticles

Features	**Graphene Nanoparticles [21]**	**Iron Oxide Nanoparticles [22]**
Thermal Conductivity (W/mK)	3000	17.65
Specific Heat (J/kgK)	790	104
Density (kg/m^3)	2250	5180
Specific Surface Area (m^2/g)	800	>80
Purity	%99.9	%99.95
Nanoparticle Size (nm)	3	14-29

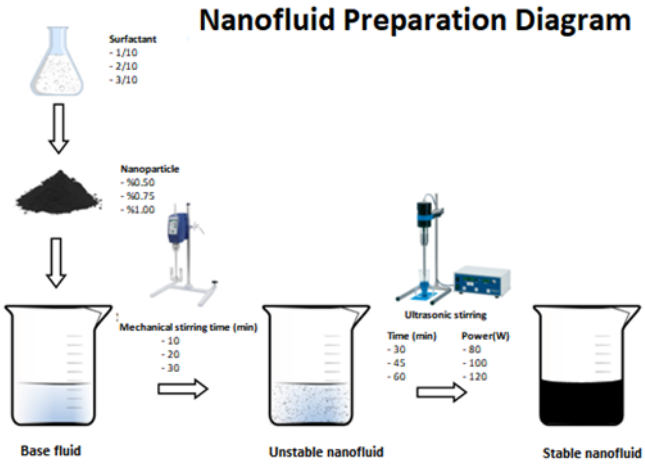


Figure 13:Nanofluid Preparation Diagram

Following the schematic shown in Figure 13, the process involved dissolving a surfactant (SDBS) [75] in 100 ml of water at a ratio of 1/10 based on the weight values of the nanoparticles determined using a precise balance (Figure 14 (e)). Subsequently, GnP-Fe_3O_4 nanoparticles were added to the base fluid equally at three different weight ratios (0.5%, 0.75%, and 1.00%). The mixture was then mechanically mixed using a mechanical mixer as depicted in Figure 13 for 30 minutes. Afterward, ultrasonic mixing was performed using a sonication device illustrated in Figure 15 (a), with a mixing power of 120 and a mixing duration of 60 minutes.

The pH level of the initial base fluid, consisting of a mixture of water and ethylene glycol, was measured using a pH meter (Figure 15 (b)) prior to the mixing process, and it was determined to be 7.28. The surfactant (SDBS) used to ensure the stability of the nanofluids has a basic nature, leading to changes in the acidity levels of the prepared nanofluids. The pH values of the nanofluids varied between 7.3 and 9.27, indicating that the acidity levels within this range do not present any potential for corrosive effects and exhibit a high potential for achieving stable nanofluids [76].

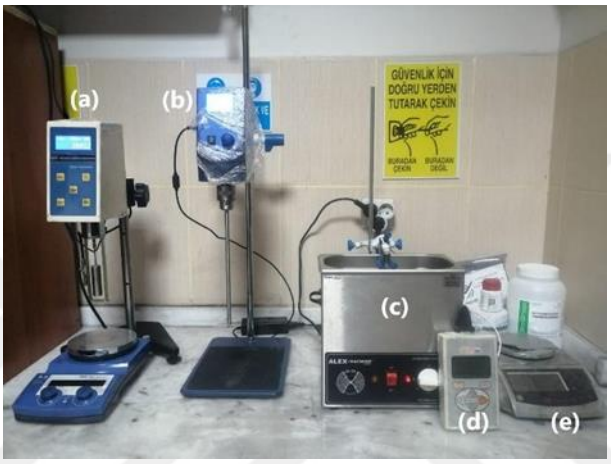


Figure 14: Nanofluid preparation and thermophysical property measurement equipment

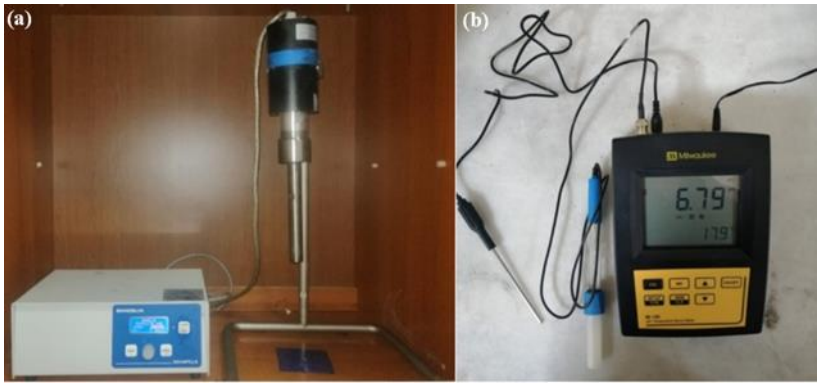


Figure 15: (a) Ultrasonic mixer and (b) pH meter

2.4. Determination of the Properties of Nanofluids

Thermal conductivity measurements were conducted using the Decagon Devices KD2 Pro thermal conductivity meter (depicted in Figure 14 (e)), while ensuring a constant temperature of the prepared nanofluid inside the ALEX brand ultrasonic water bath with a capacity of 6 L (illustrated in Figure 14 (c)), following the schematic diagram presented in Figure 16 (a). The densities and specific heat values of the nanofluids were determined through calculations using correlations derived from literature sources (Equations (1) and

(2)), while the viscosity was determined using the MRC Vis-8 rotational viscometer described in Figure 14 (a), by the schematic diagram shown in Figure 16 (b).

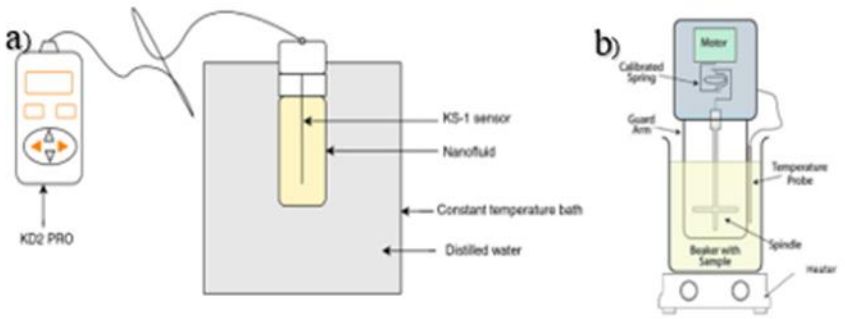


Figure 16: Thermal conductivity measurement diagram and (b) Viscosity measurement diagram [83]

$$\rho_{nf} = (1-\varphi)\rho_{bf} + \varphi\rho_{np} \quad (1)$$

$$C_{p_{nf}} = (1-\varphi)C_{p_{bf}} + \varphi C_{p_{np}} \quad (2)$$

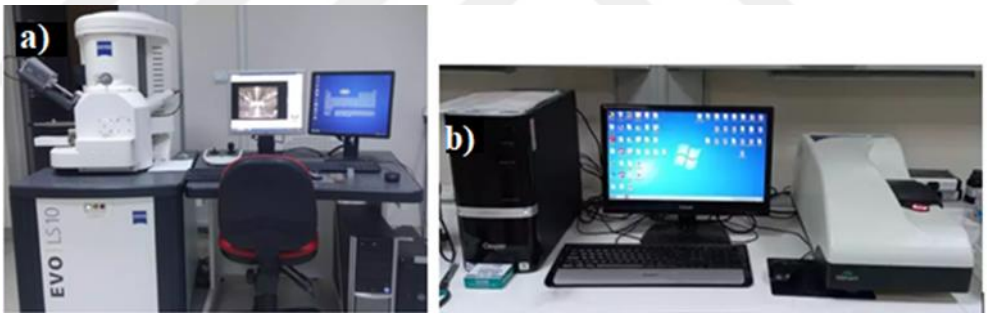


Figure 17: (a) SEM device, (b) Zeta Potential (Zetasizer) device.

SEM (Scanning Electron Microscopy) was employed at ERNAM (Erciyes University Nanotechnology Research Center) to analyze the Zeta Potential of the nanofluids prepared at various mixing ratios.

2.5. Inserts

Within the project scope, in addition to the preparation of hybrid nanofluid configurations, modified internal components (shown in Figure 18) were created by spiral-winding stainless steel wires with a circular cross-section and a diameter of 1 mm. The wires were helically wound at two different uniform distances (P=8.5 and 17 mm), while maintaining the following physical dimensions: L_e=34 mm, D_{ed}=17 mm, D_{ei}=8.5 mm, and D_e=2 mm.

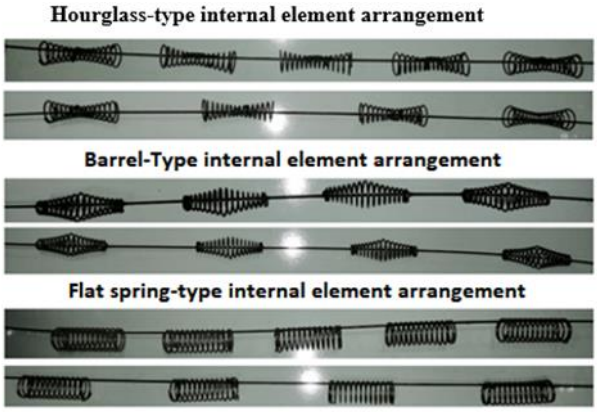


Figure 18: Configurations of internally generated components within the scope of the project

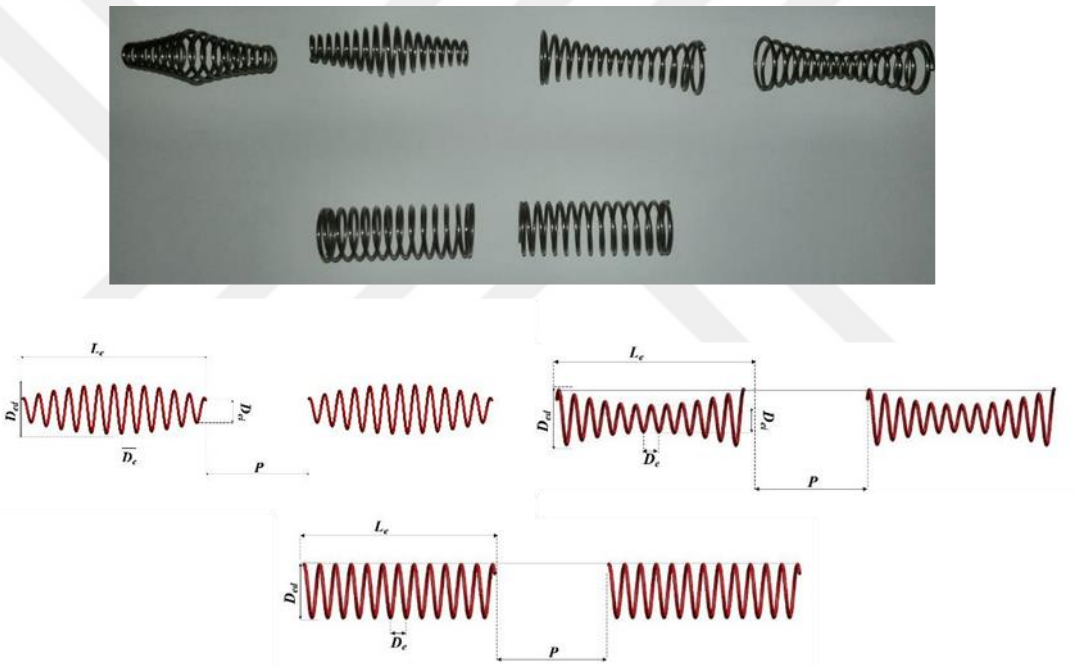


Figure 19: The internally generated components and their physical properties within the scope of the project

2.6. Calculating Dimensionless Performance Parameters

In the context of evaluating the thermal performance of a heat exchanger in a dimensionless form, the Nusselt number (Nu) is utilized, while the friction factor (f) is used to assess the hydraulic performance of the heat exchanger. Moreover, the thermo-hydraulic performance (THP) coefficient is employed to evaluate the performance of a heat exchanger in both thermal and hydraulic aspects at a specific Reynolds number (Re).

Within the project, the calculation methods for dimensionless numbers are provided below.

2.6.1. Calculating the Nusselt Number

In the experimental setup shown in Figure 20, heat is transferred through conduction from the insulation material surrounding the test tube, and heat is transferred from the insulation material to the surrounding ambient air through natural convection. The loss of heat from the experimental system to the ambient air can be calculated by determining the heat transfer value through natural convection to the ambient air. The calculation of this heat loss can be done using the equations provided below.

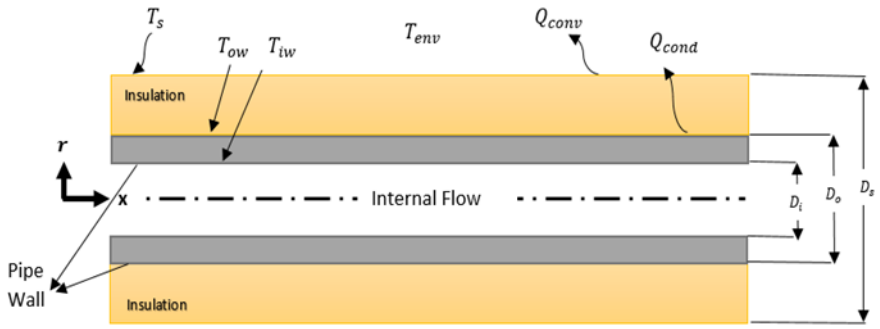


Figure 20: Cross-sectional view of the test tube.

In the calculation methodology that considers the equality between heat transfer through conduction at the insulation surface and heat transfer through convection, an iterative solution method has been developed due to the initial unknown values of the insulation surface temperature (T_s) and the external ambient heat transfer coefficient h_{env}. The heat transfer coefficient through convection is calculated using the Rayleigh number (Ra), Grashof number (Gr), and thermal expansion coefficient (β), as defined in Equations 6, 7, and 9, respectively. In these equations, the subscript "env" represents the ambient air. The thermophysical properties of air are determined based on the film temperature (T_{film}), which is the average of the insulation surface temperature and the ambient temperature, as indicated in Equation 4.

$$\dot{Q}_{con} = \dot{Q}_{fluid} \tag{3}$$

$$\frac{T_{ow} - T_s}{\frac{\ln\left(\frac{D_s}{D_o}\right)}{2\pi k_s L}} = \frac{T_s - T_{env}}{\frac{1}{h_{env}\pi D_s L}} \quad (4)$$

$$Nu_{nat} = 0.48Ra^{0.25} \quad (5)$$

$$Ra = GrPr_{env} \quad (6)$$

$$Gr = \frac{\rho_{env}\beta(T_s - T_{env})D_s^3}{\vartheta_{env}^2} \quad (7)$$

$$T_f = \frac{T_s + T_{env}}{2} \quad (8)$$

$$\beta = \frac{1}{T_{film} + 273} \quad (9)$$

$$h_{env} = k_{env}\frac{Nu_{nat}}{D_s} \quad (10)$$

The heat loss from the experimental system to the ambient air is calculated by determining h_{env} using Equation 10, as stated in Equation 11.

$$\dot{Q}_{loss} = \frac{T_{ow} - T_{env}}{\frac{\ln\left(\frac{D_s}{D_o}\right)}{k_s 2\pi L} + \frac{1}{h_{env}\pi D_s L}} \quad (11)$$

To calculate the net electrical power applied to the system (Equation 12), it is necessary to subtract the heat loss through convection from the system to the surroundings from the electrical power supplied to the system. The total electrical power supplied to the system is determined by multiplying the potential voltage difference by the current intensity. The net power is obtained by subtracting the heat loss from this power value. Dividing the net power by the surface area of the test tube gives the net heat flux (Equation 13). By evaluating the heat flux between each pair of thermal couples placed along the surface of the tube, the local heat transfer coefficient from the tube surface to the internal fluid can be calculated using Equation 14. This equation $T_{is}(x)$ represents the inner surface

temperature at a distance x and $T_b(x)$ represents the average fluid temperature within the cross-sectional area at the same distance x. The calculation methods are described below.

$$\dot{P}_{net} = \Delta V.I - \dot{Q}_{loss} \tag{12}$$

$$q^{"} = \frac{\dot{P}_{net}}{\pi D_i L} \tag{13}$$

$$h(x) = \frac{q^{"}}{T_{is}(x) - T_b(x)} \tag{14}$$

Instead of employing a temperature measurement device that would impede the flow field inside the test tube, this study successfully determined the inner wall surface temperature values by measuring the outer surface temperatures of the tube. This was accomplished by formulating a radial heat conduction equation to calculate the inner wall surface temperature values (Equation 15). This equation, P_v represents the heat generated per unit volume in the tube wall as a result of the applied electrical current, and its calculation is defined by Equation 16.

$$\frac{1}{r}.\frac{d}{dr}\left(\frac{rk_t dT}{dr}\right) = -P_v \tag{15}$$

$$P_v = \frac{P_{net}}{\frac{\pi(D_o^2 - D_i^2)L}{4}} \tag{16}$$

Boundary conditions are necessary for solving Equation 15. If boundary conditions are applied to the cross-section of the test tube,

i. $r = r_w \rightarrow -\frac{k_t dT}{dr} = 0$(Insulated Wall)

ii. $r = r_w \rightarrow T = T_{ow}(Measured\ value)$

iii. $r = r_i \rightarrow T = T_{iw}$

Through the application of these boundary conditions, Equation 17 is derived to determine the inner wall surface temperature.

$$T_{iw}(x) = T_{ow} - \frac{P_v D_o^2}{k_t}\left[\ln\left(\frac{D_o}{D_i}\right)^2 + \left(\frac{D_i}{D_o}\right)^2 - 1\right] \quad (17)$$

$$\dot{m}c_p[T_b(x) - T_b(x - \Delta x)] = \frac{P_{net}}{L}\Delta x \quad (18)$$

To calculate the average temperature of the fluid $T_b(x)$in a specific section (x), the total energy balance is applied to the fluid flowing through the heated tube of length Δx, as indicated by Equation 18.

$$T_b(x) = T_b(x - \Delta x) + \frac{\dot{P}_{net}\Delta x}{\dot{m}c_p L} \quad (19)$$

The average fluid temperature $T_b(x)$ as described in Equation 14, is calculated by applying the energy balance for the region of length Δx, as given in Equation 19. Subsequently, the local Nusselt number Nu_x is computed using Equation 20.

$$Nu(x) = \frac{h(x)D_i}{k_f} \quad (20)$$

2.6.2. Calculation of Friction Factor

The friction factor (f) is determined by measuring the pressure drop (ΔP) at the inlet and outlet pressure taps of the test tube, using Equation 3.20. In the equation, ρ_f represents the fluid density, U_m represents the average fluid velocity, L represents the distance between two points, and D_i represents the inner diameter of the tube.

$$f = \frac{\Delta P}{\frac{1}{2}\rho_f U_m^2 \frac{L}{D_i}} \quad (21)$$

2.6.3. Calculation of Thermal and Hydraulic Performance Criteria

In the conducted study, the use of both heat transfer enhancement methods, namely inserts and nanofluid utilization, leads to increased heat transfer as well as increased pressure drop. To assess the impact of these changes on the thermal system performance, the results obtained with inserts and nanofluids need to be compared to those obtained with

an empty tube and base fluid, while keeping the pumping power constant. By using constant pumping power as a reference, the evaluation of both results simultaneously is achieved through the thermal and hydraulic performance criterion (THP). The THP can be calculated using Equations 22-25 [77]. The subscripts 0 and T in the equations represent the cases where no technique is employed (empty tube and base fluid) and the cases where inserts and/or nanofluids are used, respectively.

$$\left(\dot{V}\Delta P\right)_0 = \left(\dot{V}\Delta P\right)_T \tag{22}$$

$$(fRe^3)_0 = (fRe^3)_T \tag{23}$$

$$Re_0 = Re_T \left(\frac{f_T}{f_0}\right)^{\frac{1}{3}} \tag{24}$$

$$THP = \frac{h_T}{h_0}\Big|_{pp} = \frac{Nu_T}{Nu_0}\Big|_{pp} = \left(\frac{Nu_T}{Nu_0}\right)\left(\frac{f_T}{f_0}\right)^{-1/3} \tag{25}$$

2.7. Uncertainty Analysis

The most commonly used error analysis method in the literature, proposed by Kline and Mcclintock [84], was employed to determine whether the error margins of the data obtained in the experimental study were within an acceptable range. The error values of the measurement instruments used in the preliminary study are provided in Table 2, and based on these values, the values of parameters such as Reynolds numbers, Nusselt numbers, friction coefficients, and thermohydraulic performance coefficients, which underwent uncertainty analysis, are presented in Table 3

Table 2: Error values of the measured parameters

Measured Unit	Parameters	Error Rate
Temperature	^oC	±0.75
Thermal Conductivity Coeff.	*W/mK*	± 5
Viscosity	*kg/ms*	± 1
Volumetric Flow Rate	m^3*/hour*	± 0.5
Pressure Difference	*Pa*	± 0.25
Voltage	*V*	± 3
Current	*A*	± 2

Length	m	± 0.5

Table 3: Uncertainty analysis values of the experimental data

Parameters	**Uncertainty rate %**
Reynolds number (Re)	±1.58
Nusselt number (Nu)	± 6.8
Friction Coefficient	± 2.36
Thermohydraulic performance coefficient	± 0.955

3. CHAPTER

FINDINGS

3.1. Findings Related to The Synthesis of Hybrid Nanofluids

In the study, nanofluids were prepared by incorporating Graphene-Iron Oxide nanoparticles at three different weight ratios (%0.5, 0.75, 1) into a base fluid composed of 80% pure water and 20% Ethylene glycol. The microstructures and characteristics of these nanofluid samples were determined through SEM analyses. Additionally, Zeta potential analyses were conducted to evaluate the stability of the nanofluids.

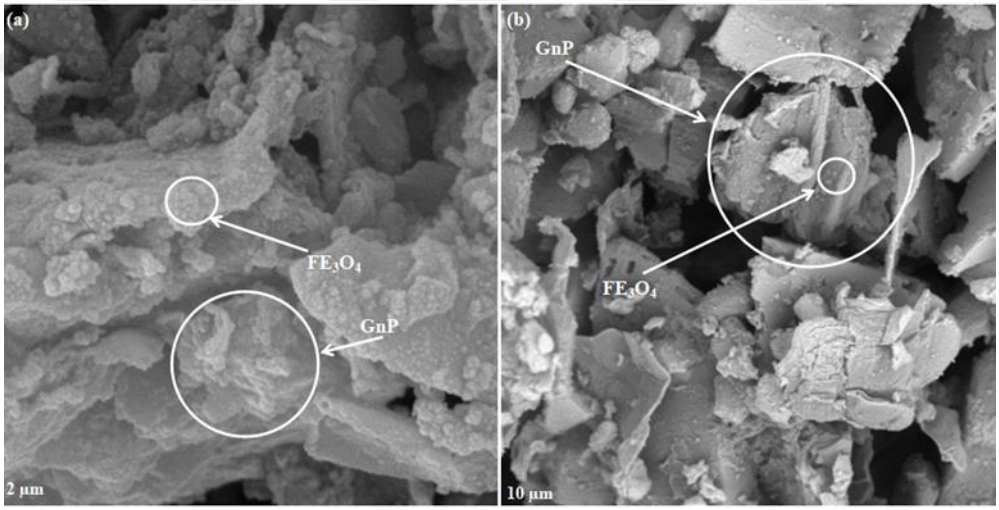


Figure 21: SEM image of graphene-iron oxide hybrid nanoparticle

As depicted in Figure 21, SEM images captured at different distances, specifically 2 µm (Figure 21(a)) and 10 µm (Figure 21(b)), illustrate Graphene nanosheets arranged in a plate-like morphology, with spherical Iron Oxide nanoparticles adhering to them. This interaction results in a nanocomposite structure that exhibits a uniform distribution. In Figure 21(a), the Iron Oxide nanoparticles densely populate the surface of the Graphene nanosheet layers, whereas Figure 21(b) provides a broader view, revealing the

distribution of Graphene nanosheets and the attachment of Iron Oxide nanoparticles onto them.

Figure 22 displays the Zeta potential analysis distributions for three different samples (%0.5, 0.75, 1). The Zeta potential values measured 11.50, 40.30, and 33.00, respectively. The corresponding results are presented in the relevant section.

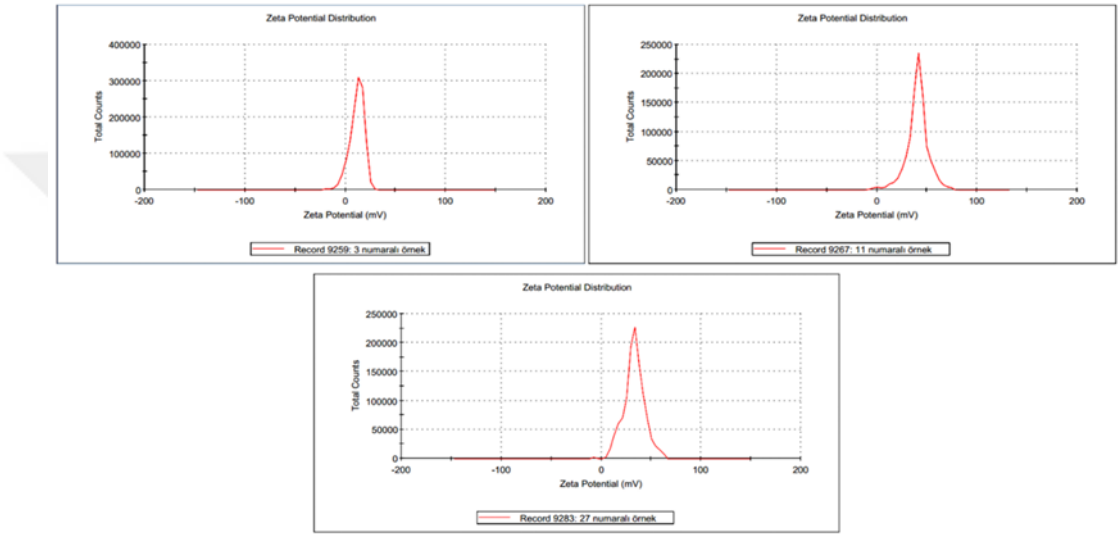


Figure 22:Zeta potential distributions of graphene-iron oxide hybrid nanoparticle

3.2. Findings on Thermophysical Properties

Following the preparation of the nanofluids, measurements of thermal conductivity and viscosity were conducted within the temperature range of 25-50°C. The density and specific heat values were calculated using commonly used Equations 26 and 27 from the literature. Initially, the thermal conductivity (Figure 23(a)) and viscosity (Figure 23(b)) values were measured for a mixture consisting of 80% pure water and 20% ethylene glycol at the specified temperatures. The measured values were then compared to the literature values, confirming the accuracy and validity of the measurement systems.

$$\rho_{nf} = (1-\varphi)\rho_{bf} + \varphi\rho_{np} \tag{26}$$

$$C_{p_{nf}} = \frac{(1-\varphi)(\rho_{bf})(C_{p_{bf}}) + (\varphi\rho_{np})(C_{p_{np}})}{\rho_{nf}} \tag{27}$$

After the verification study, the thermal conductivity coefficient and viscosity values of hybrid nanofluids were determined in the temperature range of 25-50°C. It was observed that the thermal conductivity coefficient increases with higher temperatures and higher nanofluid weight ratios. Conversely, viscosity tends to decrease with increasing temperature but increases with an increase in the nanofluid weight ratio. The highest thermal conductivity coefficient of 0.55 W/mK was achieved at 50°C for the nanofluid with a 1.00% GnP-Fe_3O_4/water-ethylene glycol composition, while the base fluid recorded a thermal conductivity coefficient of 0.50 under the same temperature conditions. The lowest viscosity value of 0.00098 kg/ms was measured at 50°C for the nanofluid with a 0.50% GnP- Fe_3O_4/water-ethylene glycol composition, compared to a viscosity value of 0.00097 kg/ms for the base fluid under the same conditions. The highest viscosity value of 0.00168 kg/ms was measured at 25°C for the nanofluid with a 1.00% GnP- Fe_3O_4/water-ethylene glycol composition, resulting in a viscosity increase of 3% compared to the base fluid configuration.

3.2.1. Regarding the Verification of the Experimental Systematic

The change in the Nusselt number (Nu) and friction factor (f) values obtained from empty tube experiments conducted with an 80% pure water-20% ethylene glycol base fluid, concerning the Reynolds number (Re), is shown in Figure 25. These experimental data were compared to the widely used Dittus & Boelter equation (28) [81] and Blasius equation (29) [82] in the literature. The experiments were carried out for five different Reynolds number values ranging from approximately 3000 to 15000. When comparing the results of the Nusselt number and friction factor with the literature, it was found that the maximum deviations were around ±11.1% and ±9.8%, respectively.

Dittus and Boelter equation:

$$Nu = 0.023 Re_D^{0.8} Pr^{0.4} \quad (28)$$

Blasius equation:

$$f = 0.316 Re_D^{-0.25} \quad (29)$$

3.2.2. Findings related to the use of hybrid nanofluid and modified inserts:

Figure 25(a) illustrates the change in Nusselt number with Reynolds number for pipe experiments conducted without the placement of inserts using the base fluid. On the other hand, Figure 26 presents the results obtained from the utilization of modified inserts within the flow area of the hybrid nanofluid at weight ratios of 0.50, 0.75, and 1.00.

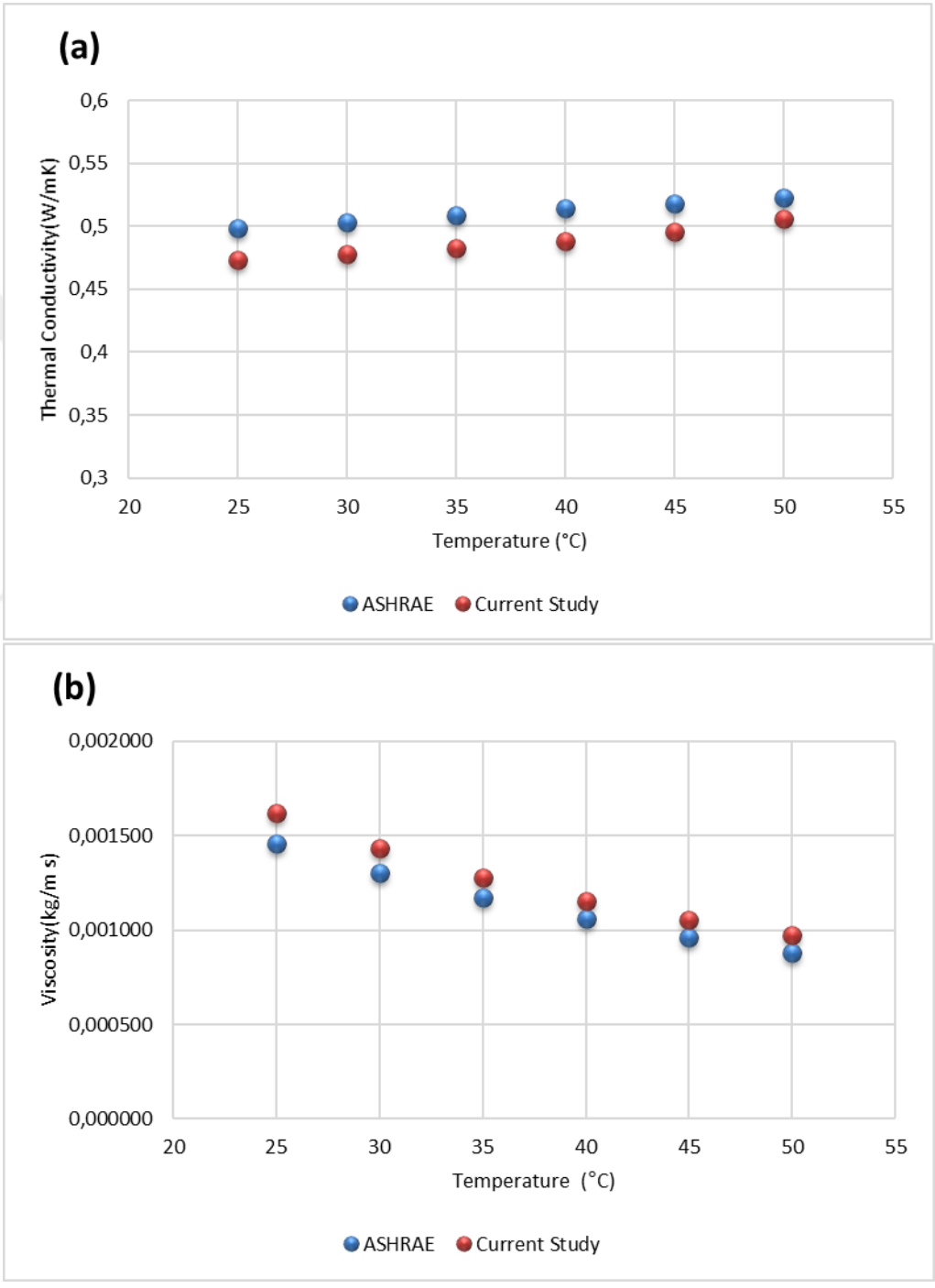


Figure 23: (a)Verification of thermal conductivity measurements (b) Verification of viscosity measurements with literature (ASHRAE [80])

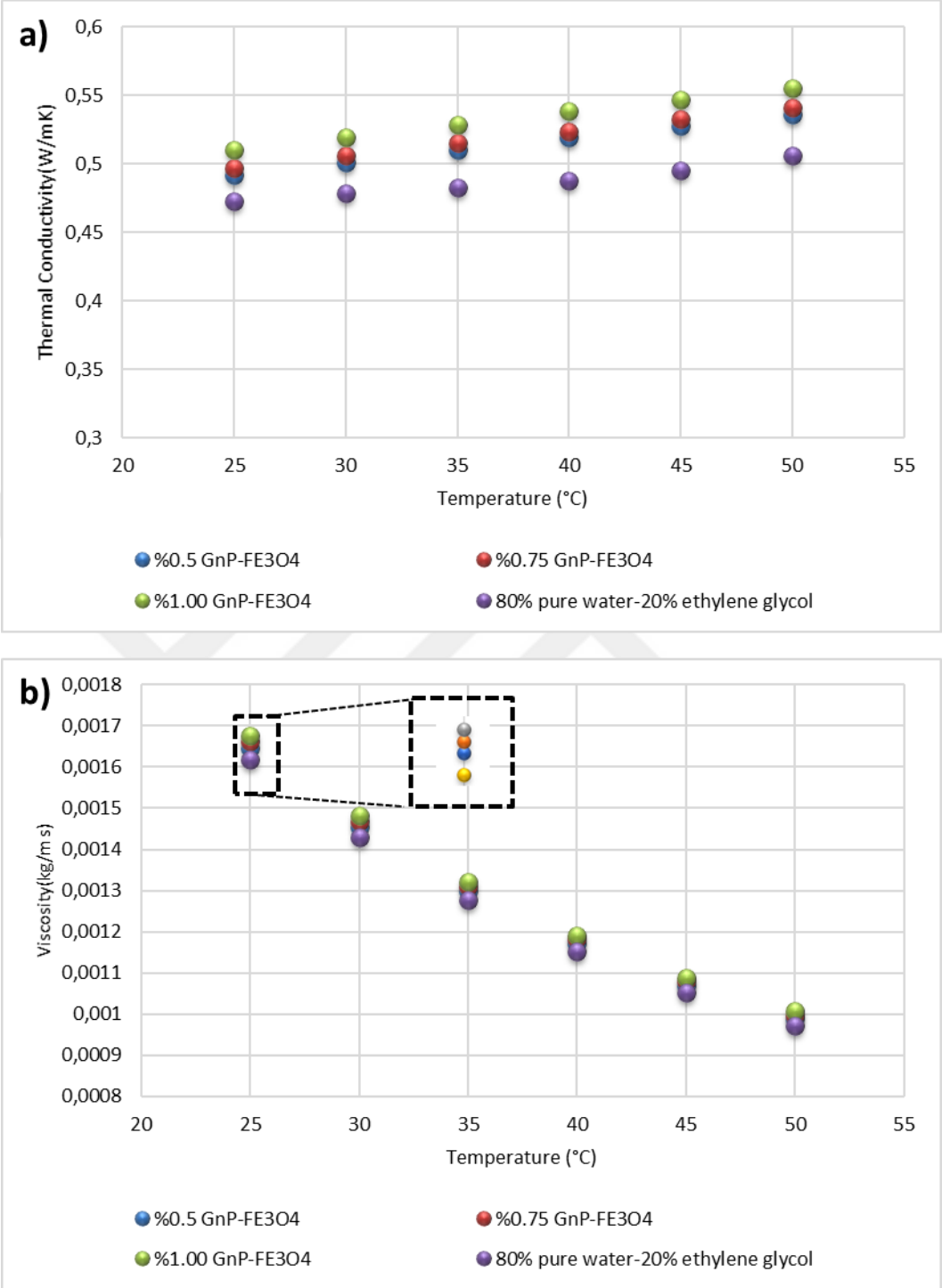


Figure 24:Variation of (a) thermal conductivity coefficients and (b) viscosity values with temperature for three different hybrid nanofluid weight ratios.

The presence of inserts in the pipe has caused an anticipated increase in the Nusselt number. These modified configurations of inserts disrupt the forms of the thermal and hydraulic boundary layers inside the pipe, promoting secondary flow and enhancing convective heat transfer, ultimately leading to an increase in the Nusselt number.

When assessing the performance of the modified inserts in terms of Nusselt number, it was observed that the barrel-type configuration provides the highest performance, followed by the hourglass-type and flat spring-type configurations. The barrel-type elements contribute to this finding by having a conducive shape for generating flow and promoting turbulence, thereby supporting secondary flow.

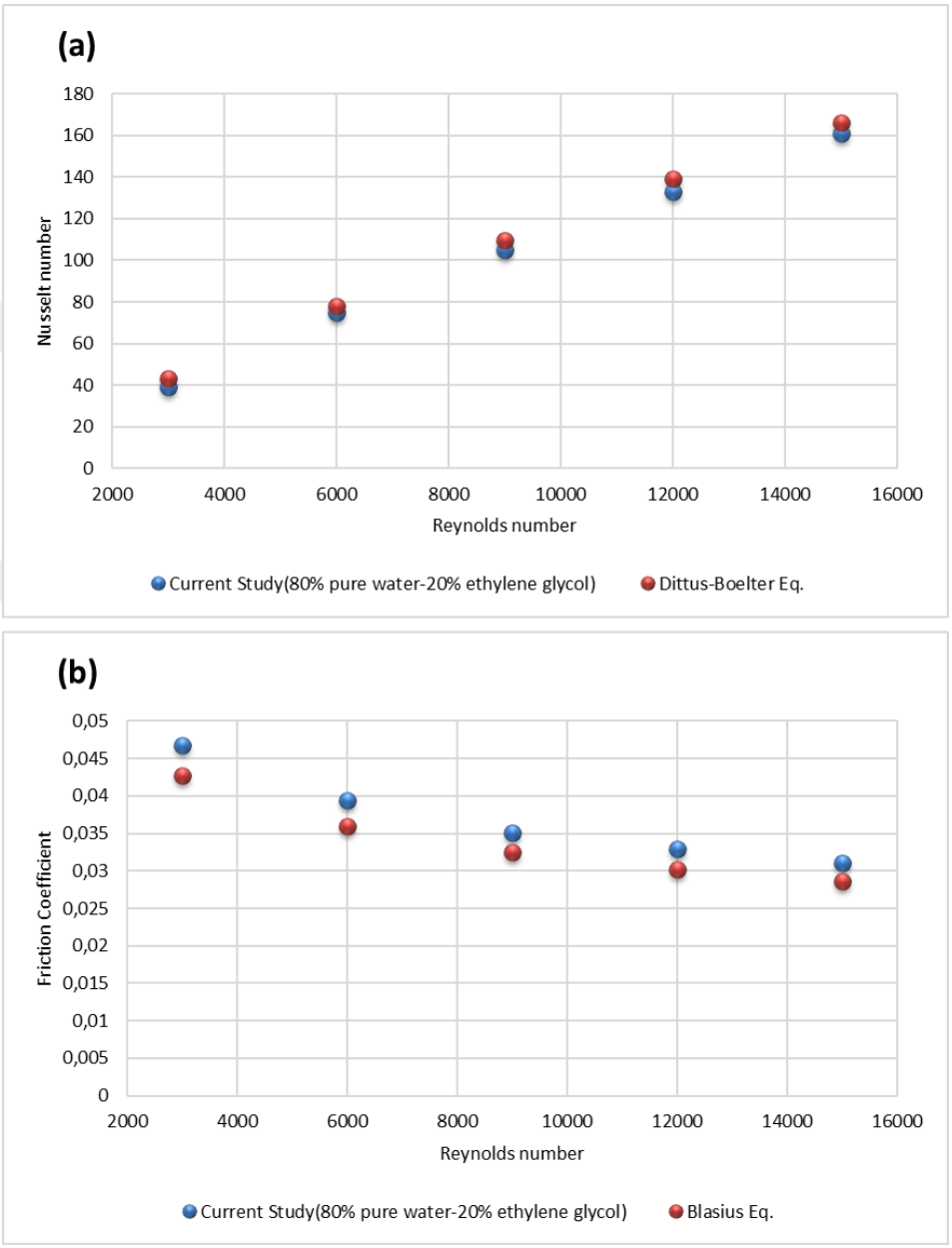


Figure 25:Comparison of the variation of (a) Nusselt number and (b) friction factor with Reynolds number obtained from empty tube experiments with the literature.

Within the individual types of modified inserts, it was noted that models with a P/D ratio of 0.5 demonstrate superior thermal performance compared to those with a P/D ratio of

1. Placing the inserts at shorter distances within the flow field leads to increased flow blockage, resulting in higher heat transfer values.

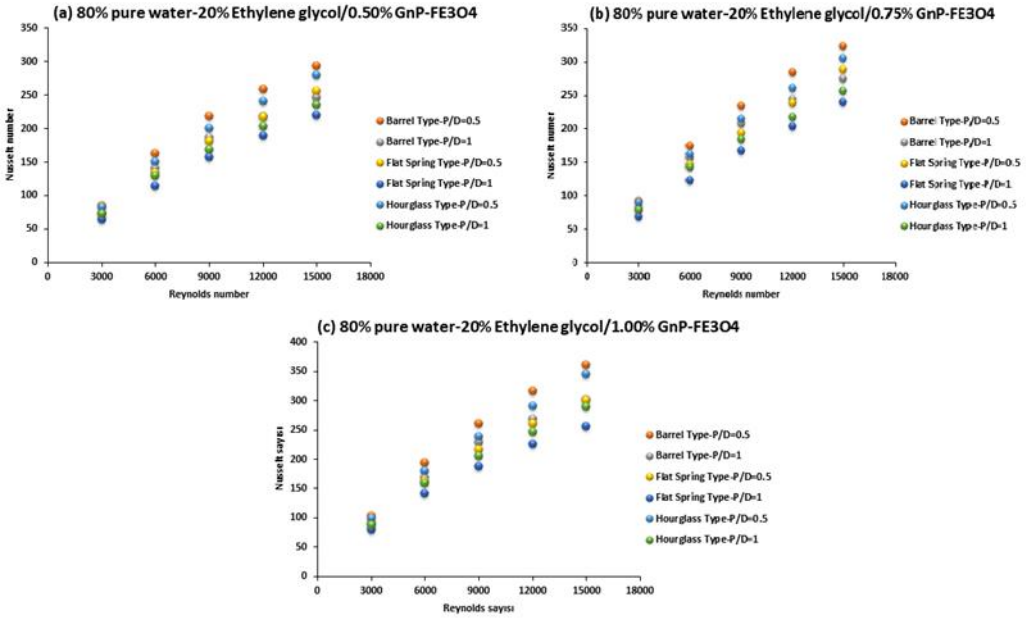


Figure 26: Distribution of Nusselt number with respect to Reynolds number for (a) 0.50%, (b) 0.75%, and (c) 1.00% hybrid nanofluid weights in insert usage.

In Figure 26, it can be observed that an increase in the hybrid nanofluid weight ratio leads to an upward trend in the Nusselt number for all insert configurations. The highest Nusselt number values were obtained when using the barrel-type insert with a P/D ratio of 0.5, regardless of the nanofluid weight ratio. Conversely, the lowest values were recorded for the flat spring-type insert with a P/D ratio of 1. Among the provided configurations, the highest Nusselt number was achieved with a %1.00 hybrid nanofluid weight ratio, a barrel-type insert with a P/D ratio of 0.5, and a Reynolds number of 15000, resulting in a value of 360. Similarly, for the %0.75 and %0.50 nanofluid weight ratios, the highest values were 323 and 293, respectively, using the same insert and Reynolds number. On the other hand, the lowest Nusselt number was observed when using the flat spring-type insert (P/D=1) at the lowest Reynolds number (3000) for all fluid models (%0.50, 0.75, and 1.00 weight ratios), with values of 63, 67, and 78, respectively.

The graphs in Figure 27 provide the relationship between the friction factor and the Reynolds number. It was found that as the nanofluid weight ratio increased, there was an increase in both pressure drop and friction factor. Compared to the empty pipe

experiments, the change in average friction factor was relatively lower compared to the increase in Nusselt number.

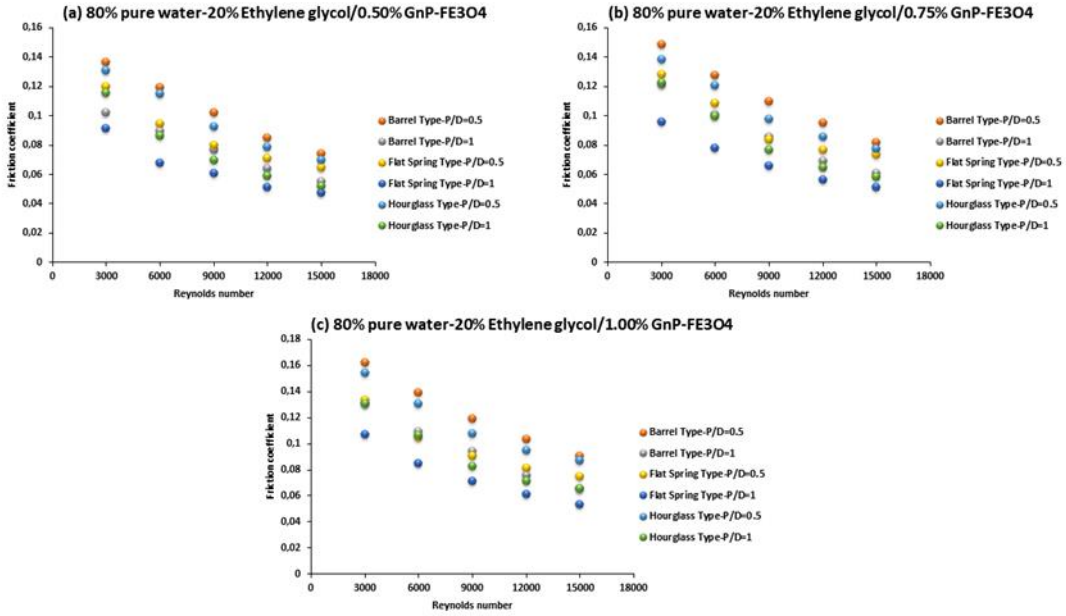


Figure 27:Distribution of friction factor with respect to Reynolds number for (a) 0.50%, (b) 0.75%, and (c) 1.00% hybrid nanofluid weights in insert usage.

All insert configurations placed inside the pipe contributed to an increase in the friction factor. This can be attributed to the modified inserts causing an increase in pressure drop along the pipe by disrupting the flow and supporting secondary flow. Evaluating the results of the inserts based on the friction factor, the barrel-type element showed the highest performance, followed by the hourglass-type and flat spring-type elements. Among the inserts, those with a P/D ratio of 0.5 exhibited better thermal performance in terms of the friction factor compared to those with a P/D ratio of 1. The closer placement of the inserts within the flow area resulted in higher levels of flow blockage, leading to higher values of heat transfer. In Figure 27(a), the highest friction coefficient for a %0.5 nanofluid weight ratio was achieved with the barrel-type element at a P/D ratio of 0.5 and Reynolds number of 3000, measuring 0.136. Similarly, for the %0.75 and %1.00 nanofluid weight ratios, the highest friction factors were obtained with the same element types and configurations, resulting in values of 0.130 and 0.120, respectively. The lowest friction factors were observed with the flat spring-type element at a P/D ratio of 1 and the lowest Reynolds number (3000), measuring 0.051 and 0.053 for the %0.75 and %1.00

nanofluid weight ratios, respectively. The friction factors showed an average increase of approximately 10% between the highest and lowest nanofluid weight ratios.

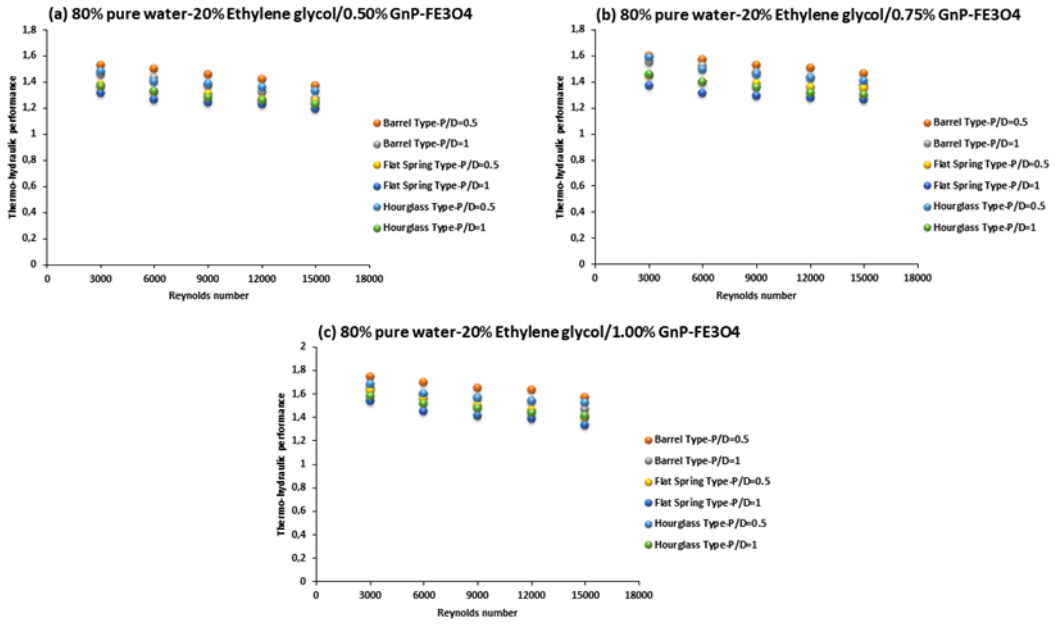


Figure 28:Distribution of thermo-hydraulic performance coefficient with respect to Reynolds number for (a) 0.50%, (b) 0.75%, and (c) 1.00% hybrid nanofluid weights in insert usage

When thermal and hydraulic performance are evaluated together in heat exchangers, the THP (Thermal Hydraulic Performance) value given in Equation 25 is commonly used. Figure 28 presents the distribution of THP values based on the Reynolds number for various insert configurations placed inside the pipe at different nanofluid weight ratios. In Figure 28(c), the pipe configuration with the barrel-type insert at a PD ratio of 0.5, which provides the best thermal performance (highest Nusselt number) and the worst hydraulic performance (highest friction factor), emerges as the most advantageous configuration when both thermal and hydraulic aspects are considered. This can be attributed to the fact that, as shown in Equation 25, the ratio of Nusselt numbers has a first-order effect on the THP value, while the ratio of friction factors has a third-order effect. In other words, while the Nusselt number offered by the pipe with inserts can be twice as high as that of an empty pipe, the friction factor can be up to eight times higher to maintain the same THP result. In short, the Nusselt number has a much greater influence on the THP value compared to the friction factor. Upon examining Figure 28, it can be observed that as the Reynolds number increases, the THP value decreases. This

is due to the increase in turbulence intensity with increasing Reynolds number, which leads to an increase in the Nusselt number. As a result, the highest THP value of 1.75 was obtained at a nanofluid weight ratio of %1.00, with the barrel-type insert at a P/D ratio of 0.5 and the lowest Reynolds number of 3000. For the %0.75 and %0.50 weight ratios, the THP values for the same configuration were 1.60 and 1.52, respectively. The lowest THP value obtained in the entire study was 1.19, achieved with the flat spring-type insert at a P/D ratio of 1 and the highest Reynolds number of 15000, with a %0.50 nanofluid weight ratio. According to these results, all configurations were considered advantageous models in terms of thermo-hydraulic performance, as the THP value exceeded 1.

4. CHAPTER

DISCUSSION-RESULT and SUGGESTIONS

4.1. Discussion

The study investigated the thermal conductivity coefficient, viscosity, and thermal-hydraulic performance (THP) of the hybrid nanofluids and the effects of modified inserts on the Nusselt number and friction factor.

The experimental results showed that the thermal conductivity coefficient of the hybrid nanofluids increased with higher temperatures and higher nanofluid weight ratios. For instance, at 50°C, the thermal conductivity coefficient of the nanofluid with a 1.00% GnP-Fe_3O_4/water-ethylene glycol composition was measured as 0.55 W/mK, while the base fluid recorded a value of 0.50 W/mK under the same temperature conditions. This indicates that the incorporation of Graphene-Iron Oxide nanoparticles into the base fluid enhanced the heat conduction capacity of the nanofluid.

The viscosity of the hybrid nanofluids displayed a complex relationship with temperature and nanofluid weight ratio. The viscosity tended to decrease with increasing temperature but increased with an increase in the nanofluid weight ratio. For example, at 50°C, the nanofluid with a 0.50% GnP- Fe_3O_4/water-ethylene glycol composition had the lowest viscosity value of 0.00098 kg/ms, compared to the base fluid value of 0.00097 kg/ms. However, at 25°C, the nanofluid with a 1.00% GnP- Fe_3O_4/water-ethylene glycol composition recorded the highest viscosity value of 0.00168 kg/ms, representing a 3% increase compared to the base fluid configuration.

The modified inserts demonstrated significant improvements in heat transfer performance compared to an empty tube setup. The Nusselt number, a dimensionless parameter

evaluating the thermal performance, increased significantly due to the presence of modified inserts. The barrel-type insert showed the highest thermal performance, followed by the hourglass-type and flat spring-type configurations. The placement of inserts at shorter distances (P/D ratio of 0.5) within the flow area led to higher heat transfer values due to increased flow blockage and enhanced turbulence.

When considering both thermal and hydraulic aspects, the THP values were calculated. The highest THP value of 1.75 was achieved at a nanofluid weight ratio of 1.00%, with the barrel-type insert at a P/D ratio of 0.5 and a Reynolds number of 3000. This indicates that this specific configuration offered the best balance between thermal enhancement and pressure drop, making it the most advantageous choice in terms of thermo-hydraulic performance.

The experimental study demonstrated that the incorporation of Graphene-Iron Oxide nanoparticles into a base fluid composed of 80% pure water and 20% ethylene glycol significantly enhanced the thermal conductivity of the nanofluids. Moreover, modified inserts placed inside the flow area effectively disrupted the thermal and hydraulic boundary layers, promoting secondary flow and improving convective heat transfer. The barrel-type insert with a P/D ratio of 0.5 showed the highest thermal performance and THP value.

These findings suggest that the use of hybrid nanofluids and modified inserts can be an effective approach to enhance heat transfer efficiency in various engineering systems. The results provide valuable insights into the potential applications of nanofluids and insert configurations to improve thermal and hydraulic performance in heat exchangers and other related systems.

4.2. Results and Suggestions

As part of the project, an experimental study was conducted to enhance passive heat transfer in a heat exchanger tube that is heated by a constant heat flux. This was achieved by introducing modified inserts of various unique configurations and preparing a hybrid nanofluid by adding GnP- Fe_3O_4 nanoparticles at different weight ratios to the base fluid, which consisted of a mixture of pure water and ethylene glycol. The experimental process

involved optimizing factors such as mechanical and ultrasonic stirring, surfactant usage, and nanofluid weight ratio to determine their effects on thermal conductivity, viscosity, and stability. The experiments were carried out under turbulent flow conditions corresponding to Reynolds numbers ranging from 3000 to 15000. The placement of all inserts and hybrid nanofluid configurations inside the heat exchanger tube contributed to improving heat transfer, and all models were found to be advantageous in terms of thermo-hydraulic performance. The configuration that exhibited the highest thermo-hydraulic performance criterion was identified as using a barrel-type insert with a P/D ratio of 0.5 and the highest weight ratio of 1.00 for the hybrid nanofluid at the lowest Reynolds number of 3000.

Increasing the weight ratio of the hybrid nanofluid leads to an observed increase in the Nusselt number. GnP and Fe_3O_4 particles have thermal conductivity values of approximately 3000 and 18 W/mK respectively, while the commonly used antifreeze configuration of 80% pure water and 20% ethylene glycol has a thermal conductivity of around 0.5 W/mK. When more nanoparticles are added, the resulting nanofluid exhibits improved thermal conductivity, allowing for enhanced heat transfer between molecules. Moreover, the nanoparticles introduce turbulence and irregularity to the flow within the tube, further accelerating heat transfer.

The friction factor, which measures flow resistance in pipe flow, is directly proportional to pressure drop and inversely proportional to flow density and velocity. Introducing nanoparticles to the base fluid increases the density and viscosity of the nanofluid. While the density increase reduces the friction factor (at the same Reynolds number), the viscosity increase raises the pressure drop, thereby increasing the friction factor. However, it is observed that the friction factor does not undergo significant changes with nanoparticle usage at the same Reynolds number.

Based on these characteristics, it can be concluded that nanofluid stability is greatly influenced. By employing different surfactant usage and mixing methods, a more stable nanofluid with higher weight ratios can be obtained, improving heat transfer performance while minimizing the increase in pressure drop and achieving higher thermo-hydraulic performance values.

Composite nanoparticles with various geometric structures, when used in the base fluid, can exhibit superior thermophysical properties compared to individual usage. Therefore, the effects of using triple hybrid composite nanoparticles with spherical, cylindrical, and plate structures on heat transfer rate and thermo-hydraulic performance can be investigated.

While the combined use of active and passive methods in heat transfer enhancement studies has become more prevalent, this study focuses on the utilization of magnetically guided nanoparticles like iron oxide in the nanofluid. By employing a combined approach of active heat transfer enhancement techniques, higher performance values can be achieved.

Inserts are commonly employed in various configurations to enhance passive heat transfer. However, their presence in thermal systems depends on the preference of system operators, and they may be removed due to contaminants. This poses a hindrance to scientific and technological advancements in energy conservation and recovery. Even with the relatively easier implementation of flat plate-type inserts, an enhancement of approximately 15% was achieved. Thus, sharing the findings and significant contributions of this scientific research with manufacturers and practitioners will greatly contribute to the desired outcomes of these studies.

REFERENCES

1. Güneli, S.S., Filimci, S., Ayğan, K., 2005. Enerji politikalarına genel bakış ve alternatif enerji politikaları. **III. Yenilenebilir enerji kaynakları sempozyumu**.
2. Ghalandari, M., Irandoost Shahrestani, M., Maleki, A., 2021. Applications of intelligent methods in various types of heat exchangers. **J Therm Anal Calorim**, **145**: 1837–1848.
3. Thulukkanam, K., 2013. Heat Exchanger Design Handbook. CRC press.
4. Shah, R.K. 1986., Classification of heat exchangers in heat exchangers. thermal hydraulic fundamentals and design. **Hemisphere Publishing Corporation**.
5. Bichkar, P., Dandgaval, O., Dalvi, P., Godase, R., & Dey, T., 2018. Study of shell and tube heat exchanger with the effect of types of baffles. **Procedia Manufacturing**, **20**: 195–200.
6. Chahartaghi, M., Eslami, P., & Naminezhad, A., 2018. Effectiveness improvement and optimization of shell-and-tube heat exchanger with entransy method. **Heat and Mass Transfer**.
7. Gut, J.A.W., Fernandes, R., Pinto, J.M., & Tadini, C.C., 2004. Thermal model validation of plate heat exchangers with generalized configurations. **Chemical Engineering Science**, **59**(21): 4591–4600.
8. Abou Elmaaty, T.M., Kabeel, A.E., & Mahgoub, M., 2017. Corrugated plate heat exchanger review. **Renewable and Sustainable Energy Reviews**, **70**: 852–860.
9. Shah, R.K. (n.d.). Extended Surface Heat Transfer. (THERMOPEDIA: **http://www.thermopedia.com/content/750/?tid=110&sn=),** (June 2023).
10. Keklikcioglu, O., Ozceyhan, V., 2018. Heat transfer models, methods and applications. In K. Volkov (Ed.): 199-217. London, InTech Open.
11. Maradiya, C., Vadher, J., & Agarwal, R., 2018. The heat transfer enhancement techniques and their thermal performance factor. **Beni-Suef University Journal of Basic and Applied Sciences**, **7**(1): 1–21.
12. Sheikholeslami, M., Gorji-Bandpy, M., & Ganji, D.D., 2015. Review of heat transfer enhancement methods: focus on passive methods using swirl flow devices. **Renewable and Sustainable Energy Reviews**, **49**: 444-469.
13. Léal, L., Miscevic, M., Lavieille, P., Amokrane, M., Pigache, F., Topin, F., Tadrist, L., 2013. An overview of heat transfer enhancement methods and new perspectives: focus on active methods using electroactive materials. **International Journal of Heat and Mass Transfer**.

14. Mousavi Ajarostaghi, S.S., Zaboli, M., Javadi, H., Badenes, B., & Urchueguia, J.F., 2022. A review of recent passive heat transfer enhancement methods. **Energies**, **15**(3): 986.

15. Thapa, S., Samir, S., Kumar, K., & Singh, S., 2021. A review study on the active methods of heat transfer enhancement in heat exchangers using electroactive and magnetic materials. **Materials Today: Proceedings**, **45**: 4942–4947.

16. Mousa, M.H., Miljkovic, N., & Nawaz, K., 2021. Review of heat transfer enhancement techniques for single-phase flows. **Renewable and Sustainable Energy Reviews**, **137**, 110566.

17. Sheikholeslami, M., Gorji-Bandpy, M., & Ganji, D.D., 2015. Review of heat transfer enhancement methods: Focus on passive methods using swirl flow devices. **Renewable and Sustainable Energy Reviews**, **49**: 444–469.

18. Léal, L., Miscevic, M., Lavieille, P., Amokrane, M., Pigache, F., Topin, F., Nogarède, B., Tadrist. L., 2013. An overview of heat transfer enhancement methods and new perspectives: focus on active methods using electroactive material. **Int. J. Heat Mass Transf**. **61**: 505–524.

19. Laohalertdecha., S., Naphon, P., Wongwises, S., 2007. A review of electrohydrodynamic enhancement of heat transfer. **Renew. Sustain. Energy Rev**. **11** (5): 858– 876.

20. Fernández, J.L., Poulter, R., 1987. Radial mass flow in electrohydrodynamically enhanced forced heat transfer in tubes**. Int. J. Heat Mass Transf**. **30** (10): 2125–2136.

21. Abadeh, A., Mohammadi, M., Passandideh-Fard, M., 2019. Experimental investigation on heat transfer enhancement for a ferrofluid in a helically coiled pipe under constant magnetic field. **J. Therm. Anal. Calorim**. **135** (2): 1069–1079.

22. Chen, C.W., Yang, C.Y., Hu, Y.T., 2013. Heat transfer enhancement of spray cooling on flat aluminum tube heat exchanger, **Heat Transf. Eng**. **34** (1): 29–36.

23. Błasiak, P., Pietrowicz, S., 2019. A numerical study on heat transfer enhancement via mechanical aids. **Int. J. Heat Mass Transf**. **140**: 203–215.

24. Hosseinian, A., Isfahani A.H.M., 2018. Experimental study of heat transfer enhancement due to the surface vibrations in a flexible double pipe heat exchanger. **Heat Mass Transf. und Stoffuebertragung 54** (4): 1113–1120.

25. Cheng, L., Luan, T., Du, W., Xu, M., 2009. Heat transfer enhancement by flow-induced vibration in heat exchangers. **Int. J. Heat Mass Transf**. **52** (3–4): 1053–1057.

26. Legay, M., Le Person, S., Gondrexon, N., Boldo, P., Bontemps, A., 2012. Performances of two heat exchangers assisted by ultrasound. **Appl. Therm. Eng**. **37**: 60–66.

27. Mousavi Ajarostaghi, S.S., Zaboli, M., Javadi, H., Badenes, B., & Urchueguia, J.F., 2022. A review of recent passive heat transfer enhancement methods. **Energies**, 15(3): 986.

28. Dewan, A., Mahanta, P., Raju, K.S., & Kumar, P.S., 2004. Review of passive heat transfer augmentation techniques. Proceedings of the Institution of Mechanical Engineers, **Part A: Journal of Power and Energy**, **218**(7): 509–527.

29. Kiwan, S., & Al-Nimr, M.A., 2001. Using porous fins for heat transfer enhancement. **Journal of Heat Transfer**, **123**(4): 790.

30. Pavel, B.I., & Mohamad, A.A., 2004. An experimental and numerical study on heat transfer enhancement for gas heat exchangers fitted with porous media. **International Journal of Heat and Mass Transfer**, **47**(23): 4939–4952.

31. Wang, B., Hong, Y., Hou, X., Xu, Z., Wang, P., Fang, X., & Ruan, X., 2015. Numerical configuration design and investigation of heat transfer enhancement in pipes filled with gradient porous materials. **Energy Conversion and Management**, **105**: 206–215.

32. Tijing, L.D., Pak, B.C., Baek, B.J., & Lee, D.H., 2006. A study on heat transfer enhancement using straight and twisted internal fin inserts. **International Communications in Heat and Mass Transfer**, **33**(6): 719–726.

33. García, A., Vicente, P.G., & Viedma, A., 2005. Experimental study of heat transfer enhancement with wire coil inserts in laminar-transition-turbulent regimes at different Prandtl numbers**. International Journal of Heat and Mass Transfer**, **48**(21-22): 4640–4651.

34. Eiamsa-ard, S., Wongcharee, K., Eiamsa-ard, P., & Thianpong, C., 2010. Heat transfer enhancement in a tube using delta-winglet twisted tape inserts. **Applied Thermal Engineering**, **30**(4): 310–318.

35. Pethkool, S., Eiamsa-ard, S., Kwankaomeng, S., & Promvonge, P., 2011. Turbulent heat transfer enhancement in a heat exchanger using helically corrugated tube. **International Communications in Heat and Mass Transfer**, **38**(3): 340–347.

36. Kareem, Z.S., Mohd Jaafar, M.N., Lazim, T.M., Abdullah, S., & AbdulWahid, A.F., 2015. Heat transfer enhancement in two-start spirally corrugated tube. **Alexandria Engineering Journal**, **54**(3): 415–422.

37. Nuntaphan, A., Vithayasai, S., Vorayos, N., Vorayos, N., & Kiatsiriroat, T., 2010. Use of oscillating heat pipe technique as an extended surface in a wire-on-tube heat exchanger for heat transfer enhancement. **International Communications in Heat and Mass Transfer**, **37**(3): 287–292.

38. Nagarani, N., Mayilsamy, K., Murugesan, A., & Kumar, G.S., 2014. Review of utilization of extended surfaces in heat transfer problems. **Renewable and Sustainable Energy Reviews**, **29**: 604–613.

39. Yadav, V., Baghel, K., Kumar, R., & Kadam, S.T., 2016. Numerical investigation of heat transfer in extended surface microchannels. **International Journal of Heat and Mass Transfer**, **93**: 612–622.

40. Bi, C., Tang, G.H., & Tao, W.Q., 2013. Heat transfer enhancement in mini-channel heat sinks with dimples and cylindrical grooves. **Applied Thermal Engineering**, **55**(1-2): 121–132.

41. Turnow, J., Kornev, N., Isaev, S., & Hassel, E., 2010. Vortex mechanism of heat transfer enhancement in a channel with spherical and oval dimples. **Heat and Mass Transfer**, **47**(3): 301–313.

42. Bianco, V., Manca, O., Nardini, S., & Vafai, K., 2017. Heat transfer enhancement with nanofluids. **CRC Press, Taylor & Francis Group**.

43. Choi, S.U.S., & Eastman, J.A. Enhancing thermal conductivity of fluids with nanoparticles. United States.

44. Xuan, Y., & Li, Q., 2000. Heat transfer enhancement of nanofluids. **International Journal of Heat and Fluid Flow**, **21**(1): 58–64.

45. Zamzamian, A., Oskouie, S.N., Doosthoseini, A., Joneidi, A., & Pazouki, M., 2011. Experimental investigation of forced convective heat transfer coefficient in nanofluids of Al2O3/EG and CuO/EG in a double pipe and plate heat exchangers under turbulent flow. **Experimental Thermal and Fluid Science**, **35**(3): 495–502.

46. Kanjirakat, A., Sadr, R., 2012. Heat Transfer Performance of SiO2-Water Nanofluid in a Plate Heat Exchanger.

47. Hussein, A.M., Bakar, R.A., Kadirgama, K., & Sharma, K.V., 2014. Heat transfer enhancement using nanofluids in an automotive cooling system. **International Communications in Heat and Mass Transfer**, **53**: 195–202.

48. Kakaç, S., Pramuanjaroenkij, A., 2009. Review of convective heat transfer enhancement with nanofluids. **International Journal of Heat and Mass Transfer**, **52**(13-14): 3187–3196.

49. Pinto, R.V., Fiorelli, F.A.S., 2016. Review of the mechanisms responsible for heat transfer enhancement using nanofluids. **Applied Thermal Engineering**, **108**: 720–739.

50. Ray, U., 2023. What are the different types of nanoparticles?. (AZoNano.com: **https://www.azonano.com/article.aspx?ArticleID=4938),** (June 2023).

51. Das, S.K., Choi, S.U.S., Patel, H.E., 2006. Heat Transfer in nanofluids—a review. **Heat Transfer Engineering**, **27**(10): 3–19.

52. Chen, J., Müller-Steinhagen, H., Duffy, G.G., 2001. Heat transfer enhancement in dimpled tubes. **Applied Thermal Engineering**, **21**(5): 535–547.

53. Piper, M., Zibart, A., Djakow, E., Springer, R., Homberg, W., Kenig, E.Y., 2019. Heat transfer enhancement in pillow-plate heat exchangers with dimpled surfaces: a numerical study. **Applied Thermal Engineering**.

54. Manikandan, S.P., Baskar, R., 2018. Assessment of the Influence of Graphene Nanoparticles on the Thermal Conductivity of Graphene/Water Nanofluids Using Factorial Design of Experiments. **Periodica Polytechnica Chemical Engineering, 62**(3): 317-322.

55. Yongsheng F., Haiqun C., Xiaoqiang S., Xin W., 2012. Combination of cobalt ferrite and graphene: high-performance and recyclable visible-light photocatalysis. **Applied Catalysis B: Environmental**, **111–112**: 280–287.

56. Oxana Vasilievna K., Beatriz Ortega G., Boris Ildusovich K., Ubaldo Ortiz M., 2016 . Magnetic-Graphene-Based nanocomposites and respective applications, Editör: Adrian M.T. Silva ve Sonia A.C. Carabineiro. London: InTech Open.

57. Guangshuo W., Yingying M., Zhiyong W., Min Q., 2016. Development of multifunctional cobalt ferrite/graphene oxide nanocomposites for magnetic resonance imaging and controlled drug delivery. **Chemical Engineering Journal**, **289**: 150–160.

58. Peng E., Choo ES., Chandrasekharan P., 2012. Synthesis of manganese ferrite/graphene oxide nanocomposites for biomedical applications. **Small**, **8**(23): 3620-3630.

59. Bhattacharyya, R., Prakash, O., Roy, S., 2019. Graphene oxide-ferrite hybrid framework as enhanced broadband absorption in gigahertz frequencies. **Sci Rep**, **9**: 12111.

60. Askari, S., Koolivand, H., Pourkhalil, M., Lotfi, R., Rashidi, A., 2017. Investigation of Fe3O4/Graphene nanohybrid heat transfer properties: experimental approach. **International Communications in Heat and Mass Transfer**, **87**: 30-39.

61. Yarman, H., Zulkifli, N., Gharehkhani, S., Shirazi, S., Alrashed, A., Azlin Bin Ali, M., Dahari, M., Kazi, S.N., 2017. Convective heat transfer enhancement with graphene nanoplatelet/platinum hybrid nanofluid. **88**: 120-125.

62. Bahiraei, M., Mazaheri, N., Hassanzamani, S.M., 2019. Efficacy of a new graphene–platinum nanofluid in tubes fitted with single and twin twisted tapes regarding counter and co-swirling flows for efficient use of energy. **International Journal of Mechanical Sciences**, **150**: 290–303.

63. Bahiraei, M., Mazaheri, N., Aliee, F., 2019. Second law analysis of a hybrid nanofluid in tubes equipped with double twisted tape inserts. **Powder Technology**, **345**: 692–703.

64. Bahiraei, M., Mazaheri, N., Rizehvandi, A., 2019. Application of a hybrid nanofluid containing graphene nanoplatelet–platinum composite powder in a

triple-tube heat exchanger equipped with inserted ribs**. Applied Thermal Engineering**, **149**: 588-601.

65. Wang, Z, Liu, C., 2015. Preparation and application of iron oxide/graphene based composites for electrochemical energy storage and energy conversion devices: Current status and perspective. **Nano Energy 11**: 277–293.

66. Lu, W., Guo, X., Yang, B., Wang, S., Liu, Y., 2019. Synthesis and applications of graphene/iron(III) oxide composites. **ChemElectroChem**, **6**: 4922 –4948.

67. Wcislik, S., 2020. Efficient Stabilization of Mono and Hybrid Nanofluids. Energies, **13**: 3793.

68. Akyürek, E.F., Geliş, K., Şahin, B., Manay, E., 2018. Experimental analysis for heat transfer of nanofluid with wire coil turbulators in a concentric tube heat exchanger. **Results in Physics**, **9**: 376–389.

69. Abdul Hamid, K., Azmi, W.H., Mamat, R., Sharma, K.V., 2019. Heat transfer performance of TiO2–SiO2 nanofluids in a tube with wire coil inserts. **Applied Thermal Engineering, 152**: 275–286.

70. Goudarzi, K., Jamali, H., 2017. Heat transfer enhancement of Al2O3-EG nanofluid in a car radiator with wire coil inserts. **Applied Thermal Engineering**, **118**: 510–517.

71. Hong, Y., Du, J., Wang, S., Huang, S., Ye, W., 2018. Heat transfer and fluid flow behaviors in a tube with modified wire coils. **International Journal of Heat and Mass Transfer**, **124**: 1347–1360.

72. Cengel, Y.A., John, C.M., 2012. Fluid Mechanics: Fundamentals and Applications. McGraw-Hill Education.

73. Choi, S.U.S., 1995. Enhancing thermal conductivity of fluids with nanoparticles. ASME FED., **231**: 99–103.

74. Kumar, A., Subudhi, S., 2019. Preparation, characterization and heat transfer analysis of nanofluids used for engine cooling. **Applied Thermal Engineering**, **160**: 114092.

75. Babita, Sharma, S.K., Gupta, S.M., 2016. Preparation and evaluation of stable nanofluids for heat transfer application: **A review. Experimental Thermal and Fluid Science**, **79**: 202–212.

76. Umar, S., Sulaiman, F., Abdullah, N., Mohamad, S.N., 2018. Investigation of the effect of pH adjustment on the stability of nanofluid. **AIP Conference Proceedings**, 020031.

77. Webb, R.L., 1981. Performance evaluation criteria for use of enhanced heat transfer surfaces in heat exchanger design. **International Journal of Heat and Mass Transfer**, **24**(4): 715–726.

78. Raghu, M.S., Kumar K., Prashanth, M.K., Prasanna, B.P., Vinuth, R., Pradeep Kumar, C.B., 2017. Adsorption and antimicrobial studies of chemically bonded magnetic graphene oxide-Fe3O4 nanocomposite for water purification. **Journal of Water Process Engineering**, **17**: 22–31.

79. Wang, Q., 2017. Preparation of high antistatic HDPE/polyaniline encapsulated graphene nanoplatelet composites by solution blending. **RSC Advances**, **7**: 2796.

80. Owen, M., (Editor) 2017. ASHRAE Handbook 2017 Fundamentals SI. American Society of Heating Refrigerating and Air-Conditioning Engineers, Atlanta, 1014.

81. Dittus, F.W., Boelter, L.M.K., 1930. Publications on engineering. University of California, Berkeley, **2**: 443.

82. Blasius, H., 1913. Das aehnlichkeitsgesetz bei reibungsvorgängen in flüssigkeiten. Mitt. Forschungsarbeiten Gebiete Ingenieurwesens, 131.

83. Yashawantha, K.M., Vinod, A.V., 2021. ANN modelling and experimental investigation on effective thermal conductivity of ethylene glycol:water nanofluids**. J Therm Anal Calorim**, **145**: 609–630.

84. Kline, S., McClintock, F., 1953. Describing Uncertainties in Single-Sample Experiments. Mechanical Engineering, pp. 3-8.

APPENDICES

APPENDIX 1.

RESUME

PERSONEL INFORMATION

Name Surname: Onur Metin MERTASLAN
Nationality: Türkiye (T.C)

EDUCATION

Degree	Institution	Graduate Date
Bachelor's degree	Abdullah Gül University, Mechanical Engineering	2020
High School	Develi İMKB Anadolu Öğretmen Lisesi, Kayseri	2015

WORK EXPERİENCES

Year	Company	Job
2022-Still	Turkish Aerospace Industry	Airworthiness Engineer

LANGUAGE

İngilizce

PUBLICATIONS

1. Atay, M. T., Mertaslan, O. M., Aca, M. K., Ylmaz, A., & Toker, B. (2020). *Haar wavelet collocation method for linear first order stiff differential equations. ITM Web of Conferences, 34, 03001*. doi:10.1051/itmconf/20203403001

2. Keklikçioğlu, O., Mertaslan, O.M., Bozkurt, M., Duman, N., İspir, M.K., & Özceyhan, V. (January 28-31, 2023). GRAFEN-DEMİR OKSİT NANOPARTİKÜLLERİ İLE OLUŞTURULAN SAF SU-ETİLEN GLİKOL BAZLI HİBRİT NANOAKIŞKANIN VİSKOZİTE ve ISIL İLETİM KATSAYISININ TESPİTİ [Conference presentation abstract]. 2nd International Conference on Innovative Academic Studies, Konya, Türkiye. https://drive.google.com/file/d/1QwAfEdWjFFaTrhVnnFRCHHvEuwwmcaZ1/view

3. Keklikcioglu, O., & Mertaslan, O.M. (20–23 June 2023). Thermohydraulic performance and second law efficiency analysis of a heat exchanger tube using a combination of two heat transfer enhancement techniques [Conference presentation abstract]. 3rd Journal of Thermal Analysis and Calorimetry Conference and 9th V4 (Joint Czech-Hungarian-Polish-Slovakian) Thermoanalytical Conference, Balatonfüred, Hungary. https://static.akcongress.com/downloads/jtacc/jtacc2023-book-of-abstracts.pdf

4. Keklikcioglu, O., & Mertaslan, O.M. (2023). Investigation the Effect of Concurrent Implementation of Hybrid Nanofluid and Modified Inserts on Thermohydraulic Performance of a Heat Exchanger Tube. Heat Transfer Research. DOI: 10.1615/HeatTransRes.2023048985